

Classification of propagation-invariant space-time wave packets in free space: Theory and experiments

Murat Yessenov, Basanta Bhaduri, H. Esat Kondakci, and Ayman F. Abouraddy
 CREOL, The College of Optics & Photonics, University of Central Florida, Orlando, FL 32816, USA
 (Dated: May 6, 2022)

Introducing correlations between the spatial and temporal degrees of freedom of a pulsed optical beam (or wave packet) can profoundly alter its propagation in free space. Indeed, appropriate spatio-temporal spectral correlations can render the wave packet propagation-invariant: the spatial *and* temporal profiles remain unchanged along the propagation axis. The spatio-temporal spectral locus of any such wave packet lies at the intersection of the light-cone with tilted spectral hyperplanes. We investigate (2+1)D ‘space-time’ propagation-invariant light sheets, and identify 10 classes categorized according to the magnitude and sign of their group velocity and the nature of their spatial spectrum – whether the low spatial frequencies are physically allowed or forbidden according to their compatibility with causal excitation and propagation. We experimentally synthesize and characterize all 10 classes using an experimental strategy capable of synthesizing space-time wave packets that incorporate arbitrary spatio-temporal spectral correlations.

I. INTRODUCTION

Optical diffraction sets universal performance limits on microscopy, lithography, and imaging, among myriad other areas. This fundamental limitation has motivated a long-standing effort for developing strategies to combat diffractive spreading by sculpting special beam profiles [1–7] (see [8], Ch. 17, for a historical perspective). Monochromatic beams having specific two-dimensional (2D) transverse spatial profiles exist that are ‘diffraction-free’ [9, 10], such as Bessel [11], Mathieu [12], Weber [13], and Airy [14] beams (see [15] for a classification). When it comes to monochromatic *one*-dimensional (1D) optical *sheets* – beams that are uniform along one transverse dimension) – *no* diffraction-free solutions exist except for the self-accelerating 1D Airy beam [16, 17].

In considering *pulsed* beams (or wave packets) having a finite spectral bandwidth, free-space propagation-invariance – diffraction-free *and* dispersion-free – has been predicted for specific spatio-temporal wave packets, including Brittingham’s focus-wave mode (FWM) [18], Mackinnon’s wave packet [19], X-waves [20–22], among other possibilities [23–28] (see [8, 29] for reviews). Underlying the propagation invariance of all these wave packets is a single fundamental principle: the *spatial* frequencies involved in the construction of the beam spatial profile must be correlated with the *temporal* frequencies underlying the pulse linewidth [30–33]. In other words, each spatial frequency (transverse component of the wave vector) is assigned to a single wavelength, thereby resulting in a spectrum incorporating strong spatio-temporal correlations. This foundational principle is in contradistinction to typical pulsed laser beams where the spectrum is approximately separable with respect to its spatial and temporal degrees of freedom. As such, the spatio-temporal spectrum for propagation-invariant wave packets occupies a *reduced-dimensionality* spectral space with respect to their traditional counterparts [33]. In light of the strong coupling between their spatial and temporal degrees of freedom, we call such propagation-invariant

pulsed beams *space-time* (ST) wave packets [32, 34]. We do not consider here scenarios in which chromatic dispersion [35–43] or optical nonlinearities [44, 45] are required for propagation-invariance, and focus solely on linear propagation in *free-space*.

We have recently demonstrated an experimental strategy for the precise synthesis of (2+1)D ST wave packets in the form of pulsed sheets with prescribed spatio-temporal correlations that can take on an arbitrary functional form [33]. Consequently, light sheets of arbitrary transverse cross-sections traveling in a straight line can now be readily synthesized. In this general methodology, each angular (temporal) frequency ω is correlated to a transverse spatial frequency k_x [32, 34], where x is the transverse coordinate. More precisely, there is a one-to-one correspondence between $|k_x|$ and ω . This correlation implies that ω and k_z are also in one-to-one correspondence, where z is the axial coordinate (the y -dependence is dropped). Making use of a spatial light modulator (SLM) to perform joint spatio-temporal spectral shaping of a femtosecond pulsed plane wave, we have demonstrated propagation-invariant ST wave packets with tailorable spatial beam profiles, including hollow [33] and *non*-accelerating Airy ST wave packets that accelerate instead in space-time [46]. Furthermore, these wave packets can be produced using refractive phase plates [47], have been shown to self-heal after scattering from opaque obstructions [48], can travel for long distances [49, 50], and can even be synthesized using broadband *incoherent* fields [51]. These recent experimental developments have stimulated several new theoretical studies of ST wave packets that examine the properties of these unique optical fields and potential approaches to their synthesis [52–57].

In this paper we present a *systematic* classification of all (2+1)D ST wave packets in which the axial wave number k_z is related *linearly* to the temporal frequency ω , $\frac{\omega}{c} = k_a + \eta k_z$, where k_a and η are real numbers, and c is the speed of light in vacuum. Such ST wave packets are particularly important because rigid translation of their spatio-temporal *envelope* is guaranteed. Furthermore, we

experimentally synthesize and characterize a representative ST wave packet from each of the identified classes. The linear correlation between k_z and ω indicates that the spatio-temporal spectra of all these ST wave packets lie along reduced-dimensionality spectral trajectories defined by the intersection of the light-cone with tilted spectral hyperplanes. We identify 10 unique classes of ST wave packets indexed with respect to three criteria: (1) the *group velocity* (subluminal, luminal, or superluminal); (2) the *direction* of the group velocity – forward or backward with respect to the source; and (3) whether *low-spatial frequencies* are allowed or forbidden, which we refer to as ‘baseband’ and ‘sideband’ ST wave packets, respectively (a nomenclature borrowed from radio engineering). A crucial advantage of the geometric picture associated with this classification is that it immediately reveals the physical limits set by causal excitation and propagation on realizable ST wave packets, a subtle issue that plagued early theoretical developments in this field [58–61]. Additionally, in one class we find a range of spatial frequencies k_x that, unexpectedly, have a two-to-one correspondence to temporal frequencies ω .

Our methodology here is close in spirit to beam synthesis in Fourier optics, and can be regarded as an embodiment of *spatio-temporal Fourier optics*. Thus, instead of realizing experimentally only specific ST wave packets whose closed-form expressions have been found, we can assign *arbitrary* complex amplitudes to the designated spatio-temporal spectral locus to synthesize *any* physically allowable ST wave packet. Indeed, many expressions for ST wave packets in the literature result from choosing particularly simple forms of the spatio-temporal spectral amplitudes, and each of these examples has – to date – required a different setup for its synthesis. Consequently, a variety of experimental arrangements have been proposed to date for the synthesis of different ST wave packets. The most salient feature of the classification presented here (compared to previous classifications [29, 31, 57]) is that it demonstrates that *all* ST wave packets can be produced via a single optical arrangement. The generality, efficiency, and systematic nature of our experimental approach is emphasized by producing realizations of *all* 10 possible classes of ST wave packets lying in any tilted spectral hyperplane utilizing the *same* setup with no moving parts – simply by changing the phase pattern displayed on a SLM.

The paper is organized as follows. First, we describe the origin of propagation invariance of an optical wave packet in the correlation between its spatial and temporal degrees of freedom. Next we present the criteria by which we classify ST wave packets before providing a detailed analysis of the 10 identified classes. We then describe our experimental methodology for synthesizing and analyzing ST wave packets, and present realizations of all 10 classes. We end the paper with a discussion of the limits of our approach and opportunities for future development, before presenting our conclusions.

II. SPATIO-TEMPORAL CORRELATIONS AS THE BASIS FOR PROPAGATION-INVARIANT SPACE-TIME WAVE PACKETS

The slowly varying envelope $\psi(x, z)$ of a scalar monochromatic fields $E(x, z, t) = \psi(x, z)e^{i(k_0 z - \omega_0 t)}$ is a solution to the paraxial equation $\{\partial_x^2 + i2k_0\partial_z\}\psi = 0$; here $k_0 = \omega_0/c$ is a fixed wave number, the *phase* velocity is $v_{ph} = c$, and we take the field distribution to be uniform along y . All such 1D beams (or sheets) diffract *except* for the 1D Airy beam [16, 17] and the trivial cases of plane and cosine waves. Finite-bandwidth *pulsed* fields $E(x, z, t) = \psi(x, z, t)e^{i(k_0 z - \omega_0 t)}$ satisfy the homogeneous, linear, scalar wave equation $\{\partial_x^2 + \partial_z^2 - \frac{1}{c^2}\partial_t^2\}E = 0$. The general solution can be expressed in a plane-wave expansion,

$$E(x, z, t) = e^{i(k_0 z - \omega_0 t)} \iint dk_x d\omega \tilde{\psi}(k_x, \omega - \omega_0) e^{i\{k_x x + (k_z - k_0)z - (\omega - \omega_0)t\}}, \quad (1)$$

where the spatio-temporal spectrum $\tilde{\psi}(k_x, \omega)$ is the 2D Fourier transform of $\psi(x, 0, t)$. Here we take k_x and ω to be the independent variables in the expansion (instead of k_z and ω , for example). This is a matter of practical convenience because k_x and ω are accessible experimentally in the course of field synthesis.

The free-space dispersion relationship $k_x^2 + k_z^2 = (\frac{\omega}{c})^2$ implied in Eq. 1 corresponds geometrically to the surface of a cone that we refer to as the ‘light-cone’, and any monochromatic plane-wave $e^{i\{k_x x + k_z z - \omega t\}}$ is represented by a point $(k_x, k_z, \frac{\omega}{c})$ on its surface. The spatial spectra of monochromatic *beams* lie on the circle at the intersection of the light-cone with the iso-frequency plane $\omega = \omega_0$ [Fig. 1(a)]. *Pulsed beams* with finite spatial *and* temporal bandwidths occupy in general a 2D patch on the surface of the light-cone [Fig. 1(b)] corresponding to the 2D spatio-temporal spectrum $\tilde{\psi}(k_x, \omega)$ in Eq. 1. Typical laser pulses separate with respect to k_x and ω ; however, exceptions in the case of high-energy pulses exist [62]. The projection onto the $(k_z, \frac{\omega}{c})$ -plane reveals that a single group velocity v_g cannot be assigned and group-velocity dispersion (GVD) is inevitable. The spatio-temporal deformation of the wave packet during propagation because of GVD is exacerbated with increased spatial and temporal bandwidths, Δk_x and $\Delta\omega$, respectively [63]. Note that decreasing Δk_x results in the spectral projection onto the $(k_x, \frac{\omega}{c})$ -plane approaching the light-line and $v_g \rightarrow c$, as expected.

A. Baseband ST wave packets with positive phase velocity

To guarantee *rigid* translation (diffraction-free *and* dispersion-free) of an ST wave-packet envelope with propagation, we adopt a reduced-dimensionality form of the field with respect to that in Eq. 1,

$$E(x, z, t) = \psi(x, z - v_g t) e^{i(k_0 z - \omega_0 t)}, \quad (2)$$

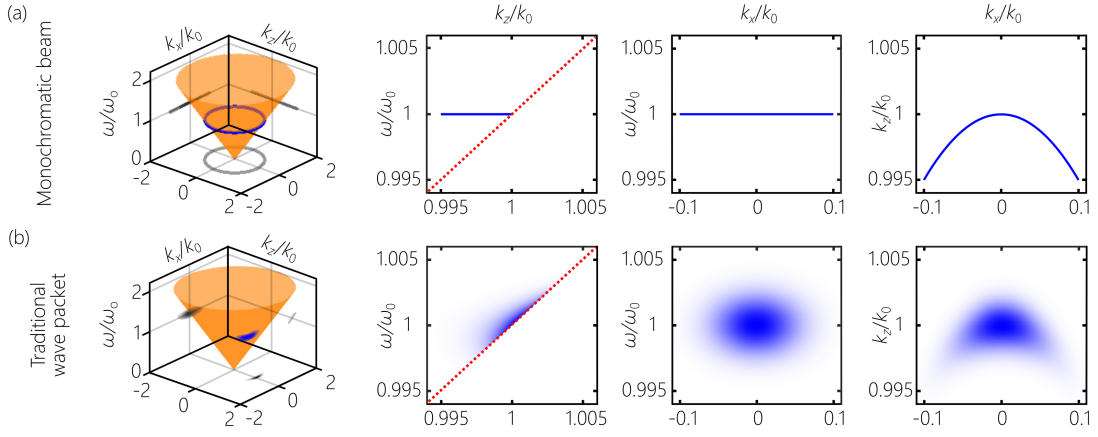


FIG. 1. Spatio-temporal spectra of traditional optical fields. (a) Monochromatic beams have spatial spectra lying at the intersection of the light-cone with the iso-frequency plane $\omega = \omega_o$, where $k_o = \frac{\omega_o}{c}$. (b) Traditional pulsed beams (wave packets) have finite spatial and temporal bandwidths, and the spatio-temporal spectrum occupies a 2D patch on the light-cone. We make use of a separable double Gaussian function, corresponding to a Gaussian spatial beam profile and Gaussian pulse linewidth, to obtain the projections in (b). In both cases we plot the projections onto the $(k_z, \frac{\omega}{c})$, $(k_x, \frac{\omega}{c})$, and (k_x, k_z) planes. The red dashed line in the $(k_z, \frac{\omega}{c})$ -plane is the light-line $\frac{\omega}{c} = k_z$.

where v_g is the *group* velocity of the ST wave packet and the *phase* velocity is $v_{ph} = \frac{\omega_o}{k_o} = c$. The reduced form of the field envelope in Eq. 2 implies in turn a plane-wave expansion of reduced dimensionality,

$$E(x, z, t) = e^{i(k_o z - \omega_o t)} \int dk_x \tilde{\psi}(k_x) e^{ik_x x} e^{i(k_z - k_o)(z - v_g t)}. \quad (3)$$

The envelope $\psi(x, z)$ is a solution to a *monochromatic* paraxial-like wave equation obtained by substituting Eq. 2 into the wave equation [30, 64],

$$\frac{\partial^2 \psi}{\partial x^2} + \left(1 - \frac{v_g^2}{c^2}\right) \frac{\partial^2 \psi}{\partial z^2} + i2k_o \left(1 - \frac{v_g}{c}\right) \frac{\partial \psi}{\partial z} = 0. \quad (4)$$

There are no *a priori* restrictions on the value of v_g . Nevertheless, we note immediately that setting $v_g = c$ does not result in a pulsed *beam*, but instead to a pulsed *plane wave*. In other words, it is impossible to construct a ST wave packet with $v_{ph} = v_g = c$ in free space. However, $v_g = -c = -v_{ph}$ is an acceptable solution for which the envelope satisfies the paraxial equation [64]

$$\frac{\partial^2 \psi}{\partial x^2} + i4k_o \frac{\partial \psi}{\partial z} = 0. \quad (5)$$

A constraint emerges from Eq. 3,

$$\frac{\omega}{c} = k_o + (k_z - k_o) \frac{v_g}{c}. \quad (6)$$

In other words, once a spatial frequency k_x is selected, the associated k_z and ω are *both* determined. Consequently, the spatio-temporal spectrum of such a wave packet does *not* occupy a 2D patch on the surface of the light-cone, such as that in Fig. 1(b), but instead lies

along a reduced dimensionality 1D curve at the intersection of the light-cone with a spectral hyperplane that is parallel to the k_x -axis and passes through the point $(k_x, k_z, \frac{\omega}{c}) = (0, k_o, k_o)$; Fig. 2(a). We denote such spectral hyperplanes $\mathcal{P}_b(\theta)$, where θ is its tilt angle to the (k_x, k_z) -plane and the subscript ‘b’ indicates that such ST wave packets are ‘baseband’ [Fig. 2(a)]; i.e., low spatial frequencies extending down to $k_x = 0$ are permissible in the field plane-wave expansion.

These curves are thus conic sections (circle, ellipse, parabola, hyperbola, or tangential line), and ω_o can be either the maximum *or* minimum frequency of the wave packet’s temporal spectrum. The projection of this curve onto the $(k_z, \frac{\omega}{c})$ -plane is in all cases a straight line passing through the point $(k_z, \frac{\omega}{c}) = (k_o, k_o)$ with a slope

$$\tan \theta = \frac{v_g}{c} = \frac{1}{n_g}, \quad (7)$$

where n_g is an effective group index. The projections of the spatio-temporal spectral curve onto the $(k_x, \frac{\omega}{c})$ and (k_x, k_z) planes are

$$\frac{1}{k_1^2} \left(\frac{\omega}{c} \pm k_2\right)^2 \pm \frac{k_x^2}{k_3^2} = 1, \quad \frac{1}{k_2^2} (k_z \pm k_1)^2 \pm \frac{k_x^2}{k_3^2} = 1, \quad (8)$$

respectively, where the signs are determined by θ as detailed below, and k_1 , k_2 , and k_3 are positive constants,

$$\frac{k_1}{k_o} = \left| \frac{\tan \theta}{1 + \tan \theta} \right|, \quad \frac{k_2}{k_o} = \frac{1}{|1 + \tan \theta|}, \quad \frac{k_3}{k_o} = \sqrt{\left| \frac{1 - \tan \theta}{1 + \tan \theta} \right|}. \quad (9)$$

We plot in Fig. 3(a) k_1 , k_2 , and k_3 with θ for subsequent reference. The relationships in Eq. 9 hold in the range $0 < \theta < \pi$, and degenerate into those for a circle at $\theta = 0$, a line at $\theta = \frac{\pi}{4}$, and a parabola at $\theta = \frac{3\pi}{4}$.

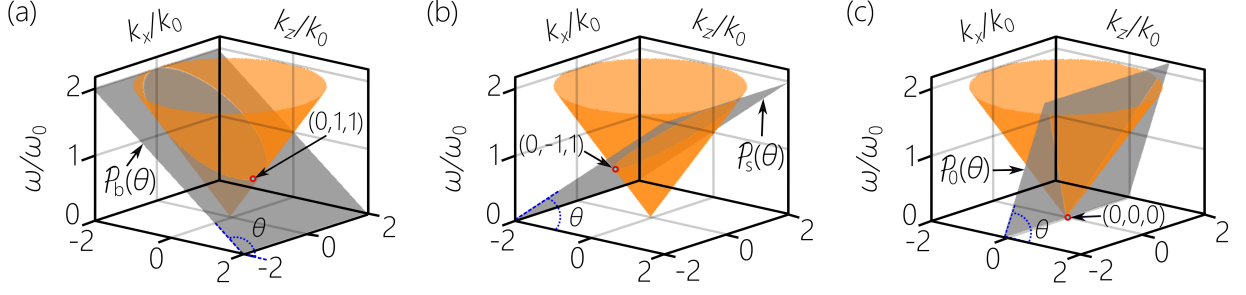


FIG. 2. Concept of ST wave packets in the spatio-temporal spectral domain. (a) *Baseband* ST wave packets. The spatio-temporal spectra lie at the intersection of the light-cone with the spectral hyperplane $\mathcal{P}_b(\theta)$ that passes through the point $(k_x, k_z, \frac{\omega}{c}) = (0, k_o, k_o)$. (b) *Sideband* ST wave packets. The spatio-temporal spectra lie at the intersection of the light-cone with the spectral hyperplane $\mathcal{P}_s(\theta)$ that passes through the point $(k_x, k_z, \frac{\omega}{c}) = (0, -k_o, k_o)$. (c) X-waves. The spatio-temporal spectra lie at the intersection of the light-cone with the spectral hyperplane $\mathcal{P}_o(\theta)$ that passes through the origin $(k_x, k_z, \frac{\omega}{c}) = (0, 0, 0)$. All hyperplanes are parallel to the k_x -axis, θ is the tilt angle with respect to the (k_x, k_z) -plane, and k_o is a fixed wave number.

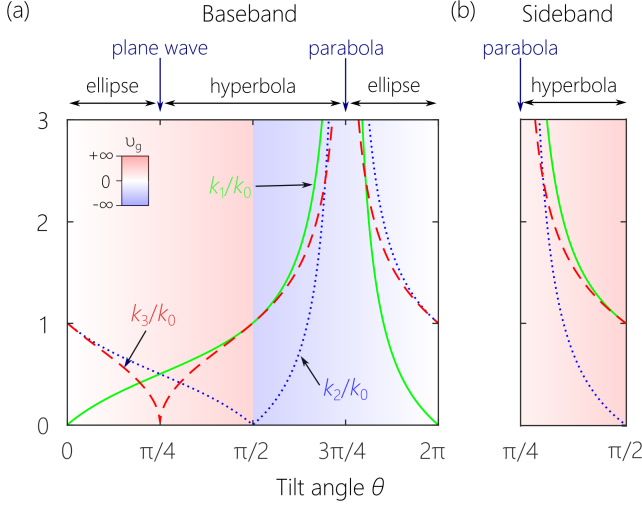


FIG. 3. (a) Plots of k_1 , k_2 , and k_3 from Eq. 9, and (b) k'_1 , k'_2 , and k'_3 from Eq. 15 as a function of θ . The background color indicates the corresponding value of v_g and the conic sections associated with the locus of the spatio-temporal spectrum are indicated at the top.

B. Sideband ST wave packets with negative phase velocity

Another form of an ST wave packet that is transported rigidly upon free propagation has $v_{ph} = -c$,

$$E(x, z, t) = \psi(x, z - v_g t) e^{-i(k_o z + \omega_o t)}. \quad (10)$$

This small change with respect to Eq. 3 has significant consequences. The reduced-dimensionality plane-wave expansion is

$$E(x, z, t) = e^{-i(k_o z + \omega_o t)} \int dk_x \tilde{\psi}(k_x) e^{ik_x x} e^{i(k_z + k_o)(z - v_g t)}. \quad (11)$$

The envelope $\psi(x, z)$ is again a solution to a monochromatic paraxial-like wave equation,

$$\frac{\partial^2 \psi}{\partial x^2} + \left(1 - \frac{v_g^2}{c^2}\right) \frac{\partial^2 \psi}{\partial z^2} + i2k_o \left(1 + \frac{v_g}{c}\right) \frac{\partial \psi}{\partial z} = 0. \quad (12)$$

Here $v_g = c$ is allowed, resulting in *luminal* sideband ST wave packets (e.g., Brittingham's FWM [18]), in which case the envelope satisfies the paraxial equation

$$\frac{\partial^2 \psi}{\partial x^2} - i4k_o \frac{\partial \psi}{\partial z} = 0. \quad (13)$$

However, $v_g = -c$ is not allowed; i.e., it is impossible to construct a free-space ST wave packet with $v_{ph} = v_g = -c$.

A new constraint emerges here from Eq. 11,

$$\frac{\omega}{c} = k_o + (k_z + k_o) \frac{v_g}{c}, \quad (14)$$

which implies that the 1D spatio-temporal spectral curve underlying the expansion in Eq. 11 lies at intersection of the light-cone with a spectral hyperplane that is parallel to the k_x -axis and passes through the point $(k_x, k_z, \frac{\omega}{c}) = (0, -k_o, k_o)$. The projection of this spectral curve onto the $(k_z, \frac{\omega}{c})$ -plane is a straight line passing through the point $(k_z, \frac{\omega}{c}) = (-k_o, k_o)$ with a slope of $\tan \theta$ as in Eq. 7. We denote such spectral hyperplanes $\mathcal{P}_s(\theta)$, where θ is its tilt angle to the (k_x, k_z) -plane and the subscript 's' indicates that such ST wave packets are 'sideband' [Fig. 2(b)]; i.e., low spatial frequencies k_x below a certain cutoff are forbidden in the field plane-wave expansion. Inclusion of lower spatial frequencies is not compatible with causal excitation, as we show below.

Planes $\mathcal{P}_s(\theta)$ intersect with the light-cone in a parabola or a hyperbola, but not an ellipse or lines. While the general forms in Eq. 8 are retained, the constants k_1 , k_2 and k_3 are replaced with a new set k'_1 , k'_2 , and k'_3 ,

respectively, where

$$\frac{k'_1}{k_o} = \left| \frac{\tan \theta}{1 - \tan \theta} \right|, \quad \frac{k'_2}{k_o} = \frac{1}{|1 - \tan \theta|}, \quad \frac{k'_3}{k_o} = \sqrt{\left| \frac{1 + \tan \theta}{1 - \tan \theta} \right|}. \quad (15)$$

For subsequent reference, we plot in Fig. 3(b) k'_1 , k'_2 , and k'_3 with θ restricted to $\frac{\pi}{4} < \theta < \frac{\pi}{2}$, which we show below is the unique range for sideband ST wave packets.

A different scenario emerges by considering $k_o \rightarrow 0$ in the intersection point of the spectral hyperplane with the light-cone, whereupon $\mathcal{P}_b(\theta)$ and $\mathcal{P}_s(\theta)$ degenerate into a plane $\mathcal{P}_o(\theta)$ that is parallel to the k_x -axis, passes through the origin $(k_x, k_z, \frac{\omega}{c}) = (0, 0, 0)$, and intersects with the light-cone in a pair of lines that meet at the origin [Fig. 2(c)]. The constraint imposed by the intersection of $\mathcal{P}_o(\theta)$ with the light-cone is

$$\frac{\omega}{c} = k_z \tan \theta, \quad (16)$$

where $\tan \theta$ is given by Eq. 7. Consequently, the plane-wave expansion takes the form

$$E(x, z, t) = \int dk_x \tilde{\psi}(k_x) e^{i\{k_x x + k_z(z - v_g t)\}}. \quad (17)$$

In *principle* the spatial spectrum can extend to include $k_x = 0$, and thus corresponds to a *baseband* ST wave packet, but this requires extending the temporal spectrum to $\omega = 0$. In *practice*, this scenario will therefore correspond to *sideband* ST wave packets. We show below that θ is restricted to the range $\frac{\pi}{4} < \theta < \frac{\pi}{2}$. The class of ST wave packets generated by $\mathcal{P}_o(\theta)$ are 1D analogs of the well-known X-waves [20–22].

C. The group velocity of ST wave packets

It is clear from the previous two subsections that v_g for ST wave packets may take on values other than c in free space [29, 65, 66]. The value of v_g is determined solely by the tilt angle θ , which is readily controlled experimentally (Sec. V) [67]. This is not a violation of special relativity; v_g is not identical to the information velocity [68]. ST wave packets can be viewed as an instance of the so-called ‘scissors effect’, whereupon the point of intersection of two very long blades of a pair of scissors can move at a considerably higher speed than that of its ears but without conveying information, or the apparent faster-than-light motion of a spotlight on a faraway screen [69]. Likewise, a negative group v_g corresponds to the closing of shears whose blades are connected at their far end: closing the shears leads to the point of the intersection of the blades to move backwards towards the source. This issue has recently been re-examined in detail by Saari [70].

III. OVERVIEW OF THE CLASSIFICATION OF SPACE-TIME WAVE PACKETS

We first present criteria for classifying ST wave packets before providing a detailed analysis in the next Section. The spectral locus of *any* ST wave packet lies at the intersection of two surfaces: the light-cone and a spectral hyperplane $\mathcal{P}_b(\theta)$, $\mathcal{P}_s(\theta)$, or $\mathcal{P}_o(\theta)$. We impose two general restrictions: (1) to avoid evanescent components, we consider only plane-wave contributions lying *on* the surface of the light-cone; and (2) we consider only *positive* (forward-propagating) values of k_z to ensure compatibility with causal excitation.

We use three criteria to classify ST wave packets:

1. *Group velocity magnitude v_g* : The linear relationship between ω and k_z results in a well-defined group velocity $v_g = \frac{\partial \omega}{\partial k_z} = c \tan \theta$, which may in principle be *subluminal* $v_g < c$, *luminal* $v_g = c$, or *superluminal* $v_g > c$.
2. *Direction of v_g* : The ST wave packet may propagate forward *away* from the source $v_g > 0$ or backward *towards* it $v_g < 0$.
3. *Baseband or sideband spatial spectra*: If the low spatial-frequency content is allowed, we refer to the ST wave packet as *baseband*, otherwise we use the term *sideband* ST wave packet, which correspond to the planes \mathcal{P}_b and \mathcal{P}_s , respectively. A third option is X-waves lying in \mathcal{P}_o , which are baseband *in principle* but sideband *in practice*.

Although $3 \times 2 \times 3 = 18$ permutations are possible, only 10 are physically realizable and unique because the two constraints eliminate several cases. For example, there are no subluminal or negative- v_g sideband ST wave packets nor subluminal X-waves. We list the physically realizable ST wave packets in Table III along with their distinguishing features. Class-1 comprises baseband positive subluminal ST wave packets $v_g < c$; Class-2 is that of baseband positive luminal ST wave packets $v_g = c$, which is a degenerate case with $k_x = 0$ (pulsed plane waves); Class-3 corresponds to baseband positive superluminal ST wave packets $v_g > c$; Class-4 is that of baseband ST wave packets formally with infinite v_g ; Class-5 is that of baseband ST wave packets with negative superluminal group velocity $|v_g| > c$; Class-6 is that of baseband negative luminal ST wave packets, $v_g = -c$; and Class-7 is that of baseband negative subluminal ST wave packets $|v_g| < c$. The remaining classes are sideband ST wave packets: Class-8 a positive luminal class $v_g = c$, and Class-9 a positive superluminal class $v_g > c$. Finally, Class-10 is that of positive superluminal X-waves [20].

TABLE I. Classification of (1+1)D ST wave packets in free space.

Class	θ	Group velocity v_g	Sign	base/side	Conic section	Name [references]
(1)	$0 < \theta < \frac{\pi}{4}$	Subluminal $v_g < c$	+ve	baseband	ellipse	Mackinnon wave packet [19]
(2)	$\theta = \frac{\pi}{4}$	Luminal $v_g = c$	+ve	baseband	line	Pulsed plane wave
(3)	$\frac{\pi}{4} < \theta < \frac{\pi}{2}$	Superluminal $v_g > c$	+ve	baseband	hyperbola	[71]
(4)	$\theta = \frac{\pi}{2}$	Superluminal $v_g = \infty$	—	baseband	iso- k_z hyperbola	[30, 32, 34, 54, 57]
(5)	$\frac{\pi}{2} < \theta < \frac{3\pi}{4}$	Superluminal $ v_g > c$	-ve	baseband	hyperbola	—
(6)	$\theta = \frac{3\pi}{4}$	Luminal $ v_g = c$	-ve	baseband	parabola	—
(7)	$\frac{3\pi}{4} < \theta < \pi$	Subluminal $ v_g < c$	-ve	baseband	ellipse	—
(8)	$\theta = \frac{\pi}{4}$	Luminal $v_g = c$	+ve	sideband	parabola	Brittingham FWM [18, 72, 73]
(9)	$\frac{\pi}{4} < \theta < \frac{\pi}{2}$	Superluminal $v_g > c$	+ve	sideband	hyperbola	—
(10)	$\frac{\pi}{4} < \theta < \frac{\pi}{2}$	Superluminal $v_g > c$	+ve	sideband	lines	X-waves [20–22]

IV. CLASSIFICATION OF SPACE-TIME WAVE PACKETS IN FREE SPACE

We describe here in detail the 10 classes of ST wave packets listed in Table III. A feature shared by *all* ST wave packets is that the projection of the spatio-temporal spectrum onto the $(k_z, \frac{\omega}{c})$ -plane is a straight line.

1. Baseband, positive subluminal ST wave packets

Such ST wave packets lie at the intersection of the light-cone with the spectral hyperplane $\mathcal{P}_b(\theta)$ in the subluminal range $0 < \theta < \frac{\pi}{4}$, where $0 < v_g < c$ and thus $n_g > 1$. The intersection is an ellipse, where ω_o is the *maximum* temporal frequency [Fig. 4(a)]. When $\theta \rightarrow 0$ close to the monochromatic limit, the ellipse tends to a circle; when $\theta \rightarrow \frac{\pi}{4}$ close to the luminal limit, the ellipse tends to a line. The projections of this ellipse onto the $(k_x, \frac{\omega}{c})$ and (k_x, k_z) planes are ellipses given by

$$\frac{1}{k_1^2} \left(\frac{\omega}{c} - k_2 \right)^2 + \frac{k_x^2}{k_3^2} = 1, \quad \frac{1}{k_2^2} (k_z - k_1)^2 + \frac{k_x^2}{k_3^2} = 1, \quad (18)$$

respectively, where k_1 , k_2 , and k_3 are defined in Eq. 9. Note that $k_1 + k_2 = k_o$, $k_2 > k_1$, and $k_2 > k_3$ [Fig. 3(a)].

The projection of the ellipse onto the $(k_x, \frac{\omega}{c})$ -plane becomes a circle at $\tan \theta = 1/\sqrt{2}$, whereupon $k_1 = k_3 = k_o/(1+\sqrt{2})$; Fig. 3(a). At smaller angles $k_1 < k_3$, while at larger angles $k_1 > k_3$, resulting in a switching of the semi-major and semi-minor axes in the $(k_x, \frac{\omega}{c})$ -plane around $\tan \theta = 1/\sqrt{2}$.

We note here a critical consequence of the constraint $k_z \geq 0$. The curvatures of the projected ellipses in the $(k_x, \frac{\omega}{c})$ and (k_x, k_z) planes in the vicinity of $k_x = 0$ have the same sign (but different magnitudes), so that a larger k_x is associated with a smaller ω and k_z . The maximum value of k_x is $|k_x^{\max}| = k_3$, corresponding to $\frac{\omega}{c} = k_2$, and thus a minimum achievable transverse spatial width is imposed on this class of ST wave packets. Further decrease in k_z is associated with a *decrease* in k_x below k_x^{\max} [Fig. 5(a)], and reaching the limit $k_z = 0$ corresponds to $k_x^0 = k_o(1 - \tan \theta)$. Consequently, the maximum temporal bandwidth is $(\Delta\omega)^{\max} = \omega_o \tan \theta$, which in turn determines a minimum achievable pulsewidth for any ST wave packet belonging to Class-1 and compatible with causal excitation. There is thus a two-to-one relationship between ω and $|k_x|$ in the range extending between k_x^{\max} and k_x^0 , a feature that is unique to Class-1. In all other classes the relationship between $|k_x|$ and ω

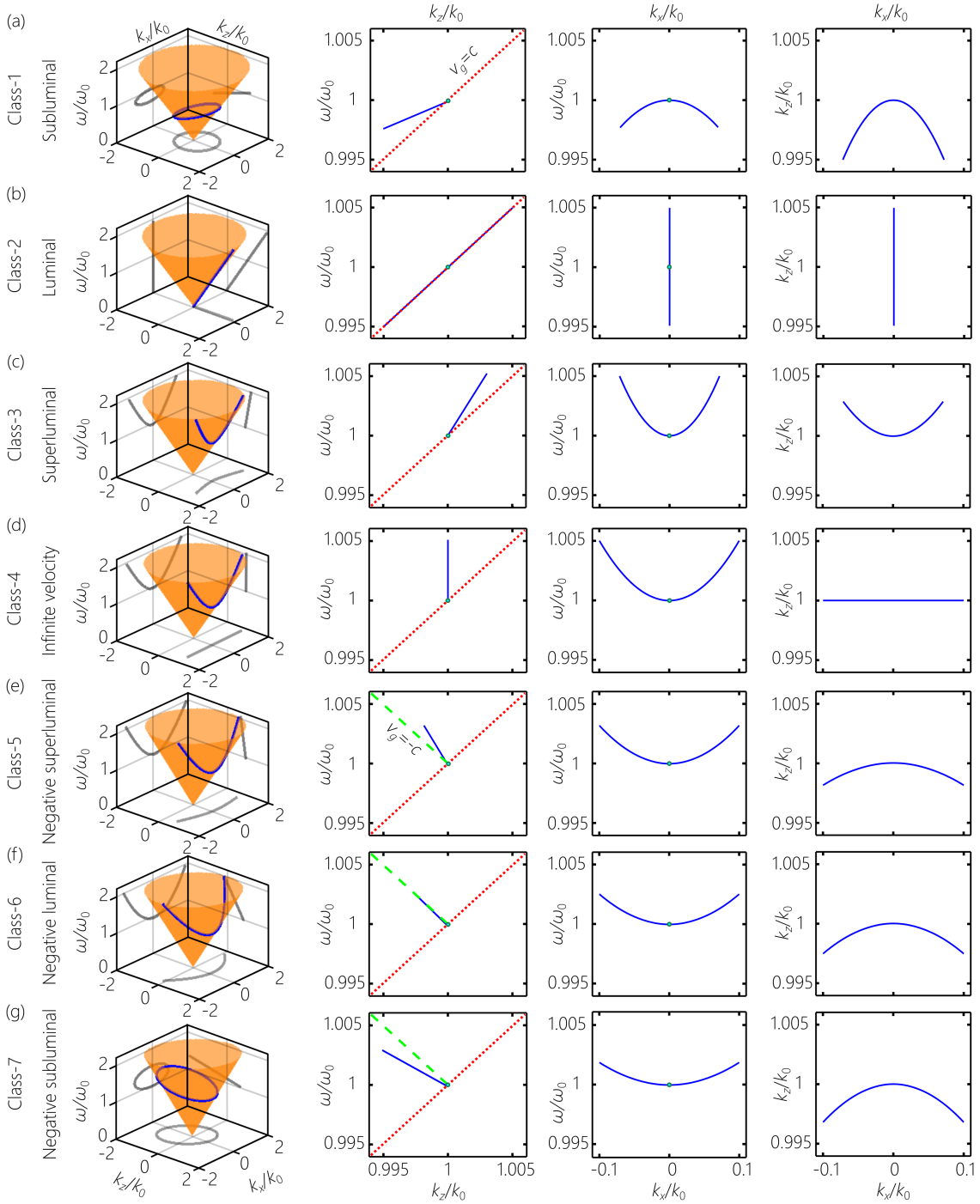


FIG. 4. Spatio-temporal spectra of *baseband* ST wave packets at the intersection of the light-cone with $\mathcal{P}_b(\theta)$ (\mathcal{P}_b itself is omitted for clarity). (a) Class-1, positive subluminal ST wave packet, $\theta = \frac{\pi}{6}$. (b) Class-2, positive luminal plane-wave pulse, $\theta = \frac{\pi}{4}$. (c) Class-3, positive superluminal ST wave packet; $\theta = \frac{\pi}{3}$. (d) Class-4, infinite- v_g ST wave packet; $\theta = \frac{\pi}{2}$. (e) Class-5, negative superluminal ST wave packet; $\theta = \frac{2\pi}{3}$. (f) Class-6, negative luminal ST wave packet; $\theta = \frac{3\pi}{4}$. (g) Class-7, negative subluminal ST wave packet; $\theta = \frac{5\pi}{6}$. The projections are idealized in the sense that they are 1D geometric curves. In practice, a finite spectral uncertainty introduced into the width of these curves is unavoidable. In all cases $\Delta k_x = 0.1k_0$. The dotted red line in the $(k_z, \frac{\omega}{c})$ -plane corresponds to $v_g = c$, and the dashed green line to $v_g = -c$.

is strictly one-to-one. These results – which are clearly gleaned from Fig. 4(a) and Fig. 5(a), but are quite sub-

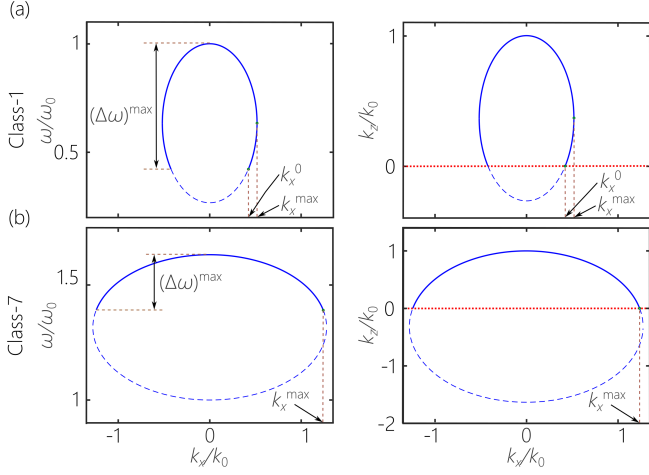


FIG. 5. Full projections on the $(k_x, \frac{\omega}{c})$ and (k_x, k_z) planes for (a) Class-1 with $\theta = 30^\circ$ and (b) Class-7 with $\theta = 166.5^\circ$. Dashed portions are excluded because they correspond to $k_z < 0$ and are thus incompatible with causal excitation and propagation. In (a) we highlight the range $k_x^0 < k_x < k_x^{\max}$ where the values of k_x are in a two-to-one relationship with ω .

tle otherwise – highlight the conceptual utility of viewing ST wave packets as resulting from the intersection of the light-cone with spectral hyperplanes. To the best of our knowledge, Class-1 ST wave packets have not been realized to date except in Ref. [33].

2. Baseband, positive luminal ST wave packets

In this case $\theta = \frac{\pi}{4}$, so that $v_g = c$ and $n_g = 1$. The plane $\mathcal{P}_b(\frac{\pi}{4})$ is tangential to the light-cone, and the intersection produces a degenerate conic section in the form of a line $\frac{\omega}{c} = k_z$ passing through the origin [Fig. 4(b)]. Consequently, this solution imposes the constraint $k_x = 0$, and Class-2 ST wave packets are pulsed *plane waves* that do not disperse in free space and naturally do not diffract, which is a well-studied model in ultrafast optics when spatial effects are neglected [63]. As mentioned earlier, it is impossible to produce a propagation-invariant wave packet of *finite* spatial extent with $v_{ph} = v_g = c$. Here ω_0 can be taken as the frequency at the center of the spectrum. Note that $k_z > 0$ for all $\omega > 0$ in this case, so that no causality-related constraints arise as did in Class-1.

3. Baseband, positive superluminal ST wave packets

For positive superluminal propagation $v_g > c$ ($n_g < 1$), $\mathcal{P}_b(\theta)$ is tilted in the range $\frac{\pi}{4} < \theta < \frac{\pi}{2}$, and intersects with the light-cone in a hyperbola, where ω_0 is now the *minimum* temporal frequency; see Fig. 4(c). The projections

onto the $(k_x, \frac{\omega}{c})$ and (k_x, k_z) planes are hyperbolas,

$$\frac{1}{k_1^2} \left(\frac{\omega}{c} - k_2 \right)^2 - \frac{k_x^2}{k_3^2} = 1, \quad \frac{1}{k_2^2} (k_z - k_1)^2 - \frac{k_x^2}{k_3^2} = 1, \quad (19)$$

respectively, where k_1 , k_2 , and k_3 are defined in Eq. 9; $k_1 + k_2 = k_0$, $k_1 > k_2$, and $k_1 > k_3$ [Fig. 3(a)]. The curvatures of these hyperbolas in the vicinity of $k_x = 0$ have the same sign but different magnitudes. Here k_1 and k_3 are the semi-major and semi-minor axes of the hyperbola, respectively in the $(k_x, \frac{\omega}{c})$ -plane, and the roles of k_1 and k_2 are then exchanged in the (k_x, k_z) -plane.

Note that $k_z > 0$ for all $\omega > 0$ and all k_x , so that no causality-related constraints arise for Class-3 as did in Class-1. In other words, there is no imposed maximum values on the spatial or temporal bandwidths, and hence no lower limit on the transverse spatial width or pulse width, except for experimental limits on the broad temporal bandwidth. An experimental arrangement to synthesize such wave packets was proposed in Ref. [71]. To the best of our knowledge, Class-3 has *not* been realized to date except in Ref. [33].

4. Baseband, infinite-group-velocity ST wave packets

In the special case $\theta = \frac{\pi}{2}$, $\mathcal{P}_b(\frac{\pi}{2})$ is a vertical iso- k_z plane $k_z = k_0$, and thus v_g is formally infinite and $n_g \rightarrow 0$. Although Class-4 is strictly speaking only a special case, we highlight it for its unique properties and because it represents the boundary between the regimes of positive- and negative- v_g . Class-4 was recently examined theoretically in Refs. [32, 34] and experimentally in Refs. [33, 46]. The plane-wave expansion in Eq. 3 simplifies for Class-3 and takes the form

$$E(x, z, t) = e^{i(k_0 z - \omega_0 t)} \int dk_x \tilde{\psi}(k_x) e^{i\{k_x x - (\omega - \omega_0)t\}}. \quad (20)$$

Therefore, the propagation of Class-4 is altogether independent of z except for an overall phase factor. The envelope is a solution to the equation

$$\frac{\partial^2 \psi}{\partial x^2} - \frac{\partial^2 \psi}{\partial (ct)^2} + i2k_0 \frac{\partial \psi}{\partial (ct)} = 0. \quad (21)$$

This is a paraxial-like wave equation, and when the second term is ignored in the slowly varying envelope approximation, we indeed retrieve the paraxial wave equation – with one difference: the axial coordinate z is replaced with time ct . Consequently, the diffractive behavior observed in the transverse *spatial* coordinate with axial propagation of a monochromatic beam having envelope $\psi(x)$ is now observed in *time* for a Class-4 ST wave packet having the same spatial spectrum. This behavior appears to have been identified initially in Ref. [30] and labeled ‘temporal diffraction’, was studied theoretically in [32] but not identified by name, and more recently investigated theoretically in [54, 57] where it has been labeled ‘time diffraction’, and experimentally in [46] where a Class-4 ST Airy wave packet was reported.

The intersection of the light-cone with $\mathcal{P}_b(\frac{\pi}{2})$ is a hyperbola whose projection onto the $(k_x, \frac{\omega}{c})$ -plane is

$$\left(\frac{\omega}{c}\right)^2 - k_x^2 = k_o^2, \quad (22)$$

while its projection in the (k_x, k_z) -plane is a straight line $k_z = k_o$ [Fig. 4(d)]. Here ω_o remains the *minimum* temporal frequency in the spectrum. The semi-major and semi-minor axes for this hyperbola are both equal to k_o . In practice, this limit is not attainable due to the unavoidable finite spectral uncertainty $\delta\omega$ in identifying the spatial and temporal frequencies, which renders v_g finite, albeit large. Finally, since $k_z = k_o > 0$ for all values of ω and k_x , there are no causality-related constraints on the transverse beam size or temporal linewidth.

5. Baseband, negative superluminal ST wave packets

When θ exceeds $\frac{\pi}{2}$, the negative slope of $\mathcal{P}_b(\theta)$ indicates a negative v_g . In the range $\frac{\pi}{2} < \theta < \frac{3\pi}{4}$, Class-5 ST wave packets are superluminal $|v_g| > c$ and travel *backwards* in the negative- z direction, corresponding to negative n_g with $|n_g| < 1$. The intersection of the light-cone with $\mathcal{P}_b(\theta)$ is a hyperbola and ω_o is the *minimum* temporal frequency. The projections onto the $(k_x, \frac{\omega}{c})$ and (k_x, k_z) planes are hyperbolas,

$$\frac{1}{k_1^2} \left(\frac{\omega}{c} + k_2\right)^2 - \frac{k_x^2}{k_3^2} = 1, \quad \frac{1}{k_2^2} (k_z - k_1)^2 - \frac{k_x^2}{k_3^2} = 1, \quad (23)$$

respectively, where k_1 , k_2 , and k_3 are defined in Eq. 9. Here we have $k_1 - k_2 = k_o$ and $k_1 > k_2$ [Fig. 3(a)]. In contrast to Class-3 and Class-4, the curvatures of the hyperbolic projections in the vicinity of $k_x = 0$ have opposite signs for Class-5 [Fig. 4(e)].

Moreover, unlike Class-3 and Class-4 that have no upper limits on the spatial and temporal bandwidths, Class-5 is characterized by upper limits on the bandwidths as a result of the inverse proportionality between ω and k_z . Increasing ω (and thus also k_x) enforces a reduction in k_z , and the restriction $k_z \geq 0$ then sets a maximal spatial frequency k_x^{\max} that is reached when $k_z = 0$,

$$|k_x^{\max}| = k_3 \sqrt{\left(\frac{k_1}{k_2}\right)^2 - 1} = k_o |1 - \tan \theta| > 2k_o, \quad (24)$$

which in turn imposes an upper limit on the temporal bandwidth,

$$(\Delta\omega)^{\max} = \omega_o |\tan \theta|. \quad (25)$$

This bandwidth corresponds to more than one octave. In other words, for a given θ , Class-5 has a *minimum* achievable spatial and temporal width that depends inversely on k_x^{\max} and $(\Delta\omega)^{\max}$, respectively. To the best of our knowledge, Class-5 has *not* been realized experimentally to date.

6. Baseband, negative luminal ST wave packets

At the negative luminal limit $\theta = \frac{3\pi}{4}$, $v_g = -c$ and $n_g = -1$. The intersection of the light-cone with $\mathcal{P}_b(\frac{3\pi}{4})$ is a parabola with ω_o corresponding to the *minimum* temporal frequency [Fig. 4(f)]. The projections onto the $(k_x, \frac{\omega}{c})$ and (k_x, k_z) planes are

$$\frac{\omega}{c} = \frac{1}{4k_o} k_x^2 + k_o, \quad k_z = -\frac{1}{4k_o} k_x^2 + k_o, \quad (26)$$

respectively. The vertex and focus of the parabola in the $(k_x, \frac{\omega}{c})$ -plane are $(0, k_o)$ and $(0, 2k_o)$, respectively, and in the (k_x, k_z) -plane are $(0, k_o)$ and $(0, 0)$, respectively. The curvatures of both these parabolas in the vicinity of $k_x = 0$ are equal in magnitude to $\frac{1}{2k_o}$, but have opposite signs [Fig. 4(f)].

Because the projected parabola in the (k_x, k_z) -plane is inverted, there is once again a *maximal* spatial frequency allowable, $|k_x^{\max}| = 2k_o$. The corresponding upper limit on the temporal bandwidth is $(\Delta\omega)^{\max} = \omega_o$, corresponding to a full octave. Therefore, there are lower limits of the spatial and temporal widths of Class-6 ST wave packets that are compatible with causal excitation. To the best of our knowledge, Class-6 has *not* been realized experimentally to date.

7. Baseband, negative subluminal ST wave packets

By further tilting $\mathcal{P}_b(\theta)$ such that $\frac{3\pi}{4} < \theta < \pi$, we reach a regime where the magnitude of the negative group velocity is subluminal $|v_g| < c$ ($n_g < -1$). The intersection of the light-cone with $\mathcal{P}_b(\theta)$ is an ellipse and ω_o is the *maximum* temporal frequency [Fig. 4(g)], in contrast to the ellipse associated with a positive subluminal v_g in Class-1 [Fig. 4(a)]. The projections onto the $(k_x, \frac{\omega}{c})$ and (k_x, k_z) planes are ellipses,

$$\frac{1}{k_1^2} \left(\frac{\omega}{c} - k_2\right)^2 + \frac{k_x^2}{k_3^2} = 1, \quad \frac{1}{k_2^2} (k_z + k_1)^2 + \frac{k_x^2}{k_3^2} = 1, \quad (27)$$

respectively, where k_1 , k_2 , and k_3 are defined in Eq. 9. Similarly to Class-5 and Class-6, the curvatures of the elliptical projections of Class-7 in the vicinity of $k_x = 0$ have opposite signs [Fig. 4(g)]. The projected ellipse in the $(k_x, \frac{\omega}{c})$ -plane becomes a circle at $\tan \theta = -1/\sqrt{2}$, whereupon $k_1 = k_3$ [Fig. 3(a)].

As in the previous two classes, the negative-slope linear relationship between ω and k_z that is responsible for the negative v_g also results in an *upper* limit of the achievable spatial and temporal bandwidths [Fig. 4(g)]. A maximum spatial frequency k_x^{\max} is associated with reaching the condition $k_z = 0$, which is given by

$$|k_x^{\max}| = k_3 \sqrt{1 - \left(\frac{k_1}{k_2}\right)^2} = k_o (1 - \tan \theta) < 2k_o. \quad (28)$$

The corresponding maximum temporal bandwidth is $(\Delta\omega)^{\max} = \omega_o |\tan \theta|$, which is *less* than one octave. Therefore there are lower limits on the achievable spatial and temporal widths of Class-7 ST wave packets. In contrast to Class-1, the one-to-one correspondence between $|k_x|$ and ω is maintained in Class-7 as shown in Fig. 5(b). To the best of our knowledge, Class-7 has *not* been realized experimentally to date.

8. Sideband, positive luminal ST wave packets

The 7 classes of *baseband* ST wave packets described thus far all lie at the intersection of the light-cone with $\mathcal{P}_b(\theta)$. We now move on to *sideband* ST wave packets resulting from the intersection of $\mathcal{P}_s(\theta)$ with the light-cone. Although $\mathcal{P}_s(\theta)$ passes through the point $(k_x, k_z, \frac{\omega}{c}) = (0, -k_o, k_o)$, we must restrict our attention to the extension of the plane along the positive half of the k_z -axis. In the subluminal range $0 < \theta < \frac{\pi}{4}$, the intersection has the form of an ellipse whose projections onto the $(k_x, \frac{\omega}{c})$ and (k_z, k_x) planes are ellipses,

$$\frac{1}{k_1'^2} \left(\frac{\omega}{c} - k_2' \right)^2 + \frac{k_x^2}{k_3'^2} = 1, \quad \frac{1}{k_2'^2} (k_z - k_1')^2 + \frac{k_x^2}{k_3'^2} = 1, \quad (29)$$

respectively, where k_1' , k_2' , and k_3' are defined in Eq. 15 [Fig. 3(b)]. However, these ellipses are *not* unique and in fact coincide with those of Class-1, which can be confirmed by making the substitution

$$k_o \rightarrow k_o \frac{1 + \tan \theta}{1 - \tan \theta}, \quad (30)$$

in which case the ellipses in Eq. 18 are retrieved. We thus do *not* identify this case as a unique class.

In the positive luminal case of $\theta = \frac{\pi}{4}$, whereupon $v_g = c$ and $n_g = 1$, $\mathcal{P}_s(\frac{\pi}{4})$ intersects the light-cone in a parabola with a *minimum* temporal frequency of $2\omega_o$. The projections onto the $(k_x, \frac{\omega}{c})$ and (k_x, k_z) planes are parabolas,

$$\frac{\omega}{c} = \frac{1}{4k_o} k_x^2 + k_o, \quad k_z = \frac{1}{4k_o} k_x^2 - k_o, \quad (31)$$

respectively. The vertex and focus of the parabola in the $(\frac{\omega}{c}, k_x)$ -plane are $(0, -k_o)$ and $(0, 0)$, respectively, and in the (k_x, k_z) -plane are $(0, k_o)$ and $(0, 2k_o)$, respectively.

As shown in Fig. 6(a), the low-frequency range in the vicinity of $k_x = 0$ is excluded since it corresponds to $k_z < 0$. The *minimum* allowed value of k_x associated with $k_z = 0$ is $|k_x^{\min}| = 2k_o$. Beyond the minimum values, there are no *upper* limits on the spatial or temporal frequencies. Therefore, arbitrary spatial and temporal widths of Class-8 ST wave packets are achievable, with the caveat that the *low* spatial frequencies below k_x^{\min} are excluded. The well-known example of Brittingham's FWM [18] belongs to Class-8. An optical arrangement for synthesizing such wave packets was proposed in [72] and initial experimental results indicating its feasibility in the optical domain were reported in [73].

9. Sideband, positive superluminal ST wave packets

In the positive superluminal range $\frac{\pi}{4} < \theta < \frac{\pi}{2}$, whereupon $v_g > c$ and $n_g < 1$, $\mathcal{P}_s(\theta)$ intersects with the light-cone in a hyperbola; $(1 + \tan \theta)\omega_o$ is the *minimum* temporal frequency. The projections onto the $(k_x, \frac{\omega}{c})$ and (k_x, k_z) planes are hyperbolas,

$$\frac{1}{k_1'^2} \left(\frac{\omega}{c} + k_2' \right)^2 - \frac{k_x^2}{k_3'^2} = 1, \quad \frac{1}{k_2'^2} (k_z + k_1')^2 - \frac{k_x^2}{k_3'^2} = 1, \quad (32)$$

respectively, where k_1' , k_2' , and k_3' are defined in Eq. 15 [Fig. 3(b)]; $k_1' - k_2' = k_o$ and $k_1' > k_2'$. The minimum value of k_x for Class-9, corresponding to $k_z = 0$, is

$$|k_x^{\min}| = k_3' \sqrt{\left(\frac{k_1'}{k_2'} \right)^2 - 1} = k_o (1 + \tan \theta) = \left(\frac{\omega}{c} \right)^{\min}. \quad (33)$$

Similarly to Class-8, beyond these minimum values, there are no upper limits on the spatial and temporal frequencies for Class-9. Therefore, arbitrary spatial and temporal widths are achievable in Class-9 once the low spatial frequencies below k_x^{\min} are excluded. To the best of our knowledge, Class-9 has *not* been synthesized experimentally to date.

10. Positive superluminal X-wave ST wave packets

X-waves [20–22] are ST wave packets whose spatio-temporal spectra lie at the intersection of $\mathcal{P}_o(\theta)$ with the light-cone in the superluminal range $\frac{\pi}{4} < \theta < \frac{\pi}{2}$. These intersections take the form of a pair of lines whose projections onto the $(k_x, \frac{\omega}{c})$ and (k_x, k_z) planes are

$$\frac{\omega}{c} = \frac{k_x \tan \theta}{\sqrt{\tan^2 \theta - 1}}, \quad k_z = \frac{k_x}{\sqrt{\tan^2 \theta - 1}}, \quad (34)$$

respectively. As mentioned earlier, although Class-10 is formally baseband since the low-frequency portion of the spatial spectrum is not excluded, such ST wave packets are in practice of the sideband family because $k_x = 0$ corresponds to the DC frequency $\omega = 0$. Whereas previous experiments on synthesizing optical X-waves realized 2D spatial profiles [22], there have been no demonstrations to date of 1D X-waves in Class-10. There are no limits beyond experimental restrictions on the achievable spatial and temporal bandwidths, and thus no lower limits on the minimum spatial or temporal widths.

V. GENERATION OF SPACE-TIME WAVE PACKETS

The experimental strategy that we adopt is based on ultrafast pulse-shaping via spectral phase modulation [74, 75]. However, in lieu of a 1D SLM modulating the phase of the temporal spectrum, we utilize a 2D phase

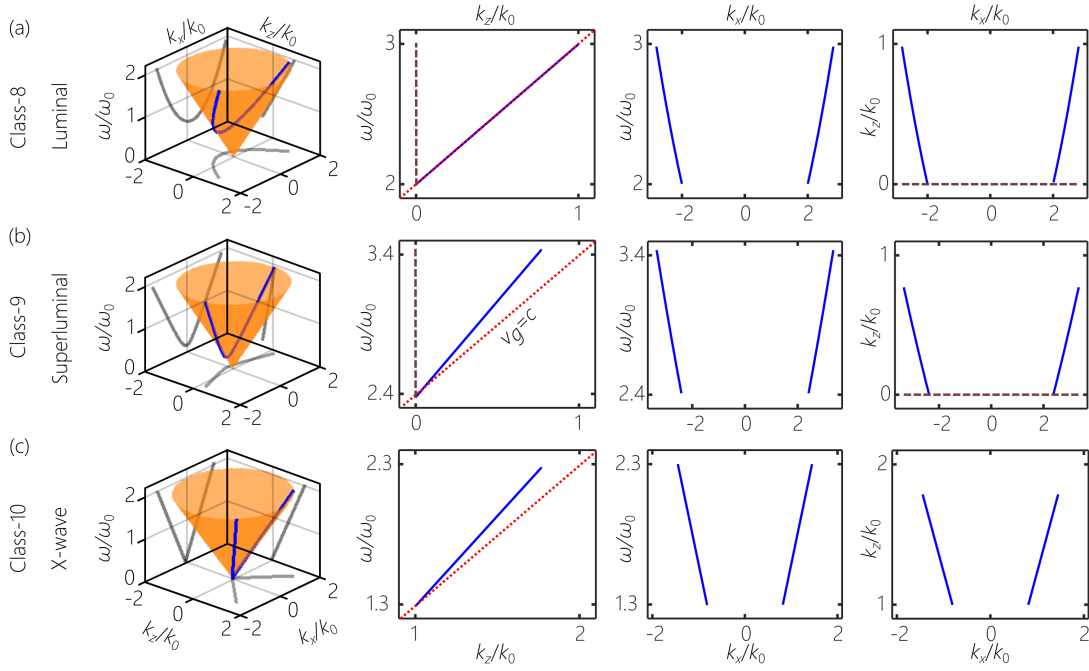


FIG. 6. *Sideband* ST wave packets resulting from the intersection of the light-cone with plane $\mathcal{P}_s(\theta)$ (\mathcal{P}_s itself is omitted for clarity). (a) Class-8, positive luminal ST wave packet; $\theta = \frac{\pi}{4}$. (b) Class-9, positive superluminal ST wave packet; $\theta = \frac{3\pi}{10}$. (c) Class-10, positive superluminal ST wave packets (X-waves) resulting from the intersection of the light-cone with $\mathcal{P}_o(\theta)$; $\theta = \frac{2.89\pi}{10}$. The dotted red line in the $(k_z, \frac{\omega}{c})$ -plane corresponds to $v_g = c$, and the dashed black line to $k_z = 0$.

modulation scheme where the dimension orthogonal to the temporal spectrum is exploited to introduce a spatial frequency k_x associated with each temporal frequency or wavelength λ [76–81]. The critical advantage of this scheme is that it allows for programming an arbitrary correlation function between λ and k_x , in principle following those associated with *any* of the classes of ST wave packets described above and listed in Table III. This is accomplished simply by implementing the appropriate 2D phase modulation on the SLM that corresponds to the projection onto the $(k_x, \frac{\omega}{c})$ -plane of the spatio-temporal spectral curve of the desired ST wave packet.

A. Experimental setup

1. Synthesis of ST wave packets

Figure 7(a) depicts schematically the experimental setup utilized in synthesizing ST wave packets. This is essentially an ultrafast pulse-shaping setup with spatial beam modulation implemented simultaneously. A horizontally polarized large-area femtosecond pulsed beam from a Ti:Sa laser (Tsunami, Spectra Physics; bandwidth of ~ 8.5 nm centered on a wavelength of ~ 800 nm) is directed at an incidence angle of 68.5° to a reflective diffraction grating G having 1200-lines/mm ruling and an area of 25×25 mm² (Newport 10HG1200-800-1). The reflected

spectrum is directed through a cylindrical lens L_{1-y} (focal length $f = 50$ cm) oriented along the y -direction in a $2f$ configuration to collimate the pulse spectrum in space. By selecting the second diffraction order, the parameters utilized in the experiment allow for a temporal bandwidth of ~ 2.1 nm from the input laser to spread over the full transverse width ~ 16 mm of a reflecting phase-only SLM (Hamamatsu X10468-02) that modulates the impinging wave front with a 2D spatial phase $\Phi(x, y)$.

To produce a representative from each of the 10 classes of ST wave packets, only an appropriate phase pattern need be displayed on the SLM [Figs. 8-10]. After spreading the temporal spectrum in space, each column of the SLM modulates a particular wavelength, and we introduce in that column a linearly varying phase whose slope corresponds to a specific spatial frequency k_x . A programmable one-to-one correspondence between $|k_x|$ and λ can thus be enforced. The phase-modulated wavefront is retro-reflected back through the lens L_{1-y} to the grating G. The pulse is reconstituted by superposing all the wavelengths, and as a consequence of the correlation between spatial and temporal frequencies, the spatial frequencies are simultaneously superposed – thereby producing the ST wave packet in the form of a light sheet.

For the sake of comparison, we also make use of the experimental arrangement, after introducing the modifications shown in Fig. 7(b), to produce a monochromatic beam and also a traditional pulsed beam in which

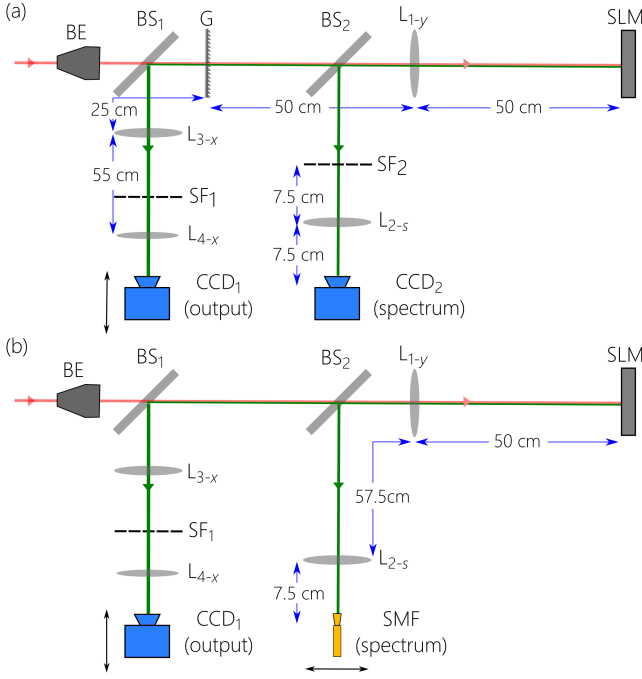


FIG. 7. Schematic depiction of the experimental setup to synthesize and characterize (a) ST wave packets; (b) monochromatic and traditional pulsed beams. BE: Beam expander; BS₁, BS₂: beam splitters; G: diffraction grating; CCD₁, CCD₂: CCD cameras; SLM: spatial light modulator; SMF: single mode fiber; SF₁, SF₂: spatial filters; L_{1-y}, L_{3-x}, L_{4-x}: cylindrical lenses; L_{2-s}: spherical lens. The focal lengths of all the lenses and their separations are given in the figure.

the spatial and temporal spectra are *uncoupled*. The major difference in the synthesis portion of the setup is that the diffraction grating G is removed, such that the initial beam – whether monochromatic or pulsed – is incident on the SLM without first spreading the temporal spectrum. The spatial frequencies are then assigned to the *whole* temporal spectrum (and not each to a single wavelength as in the case of ST wave packets), thus resulting in a separable spatio-temporal spectrum. Therefore, despite having the same spatial bandwidth, the ST wave packets are expected to be diffraction-free as a result of the spatio-temporal spectral correlations, whereas the monochromatic and pulsed beams having uncoupled spatio-temporal spectra are expected to undergo the usual diffractive spreading.

2. Design of the SLM phase distribution $\Phi(x, y)$

The usage of an SLM to implement the desired spatio-temporal spectral correlations imposes several limitations. The total width of the SLM determines the useful bandwidth, and the finite size of the SLM pixels determines the spectral uncertainty $\delta\lambda$ associated with the identification of a wavelength λ to a specific spatial fre-

quency k_x . In addition, the ratio of the SLM total width to the pixel width determines the highest implementable k_x along the direction orthogonal to the spread spectrum. To maximize the utilization of the SLM, we make use of phase distributions $\Phi(x, y)$ in which the spatial frequencies are *reduced* by a factor of $10\times$ when synthesizing any of the 7 baseband ST wave packets (a factor of $100\times$ was used with sideband ST wave packets because of the higher spatial frequencies involved). In other words, each λ is associated *not* with the correctly designed spatial frequency k_x , but instead with $k_x/10$. At the final stage of ST wave packet synthesis after the pulsed beam is reconstituted by the diffraction grating G, we ‘amplify’ the spatial spectrum via two cylindrical lenses L_{3-x} ($f = 50$ cm) and L_{4-x} ($f = 5$ cm) oriented along the x -direction that introduce a demagnification of $10\times$ when synthesizing baseband ST wave packets; see Fig. 7. As a result, each k_x is replaced with $10k_x$ at this step, and the overall result is to produce the intended correlation function between λ and k_x .

Note that only a flat phase distribution $\Phi(x, y) = \text{constant}$ is needed to synthesize Class-2 ST wave packets that correspond in the spatial domain to a plane wave.

3. Measuring the ST wave packet evolution in physical space

To characterize the ST wave packet in physical space, the reconstituted pulsed beam after G is directed by a beam splitter BS₁ to a two-lens telescope system consisting of cylindrical lenses L_{3-x} and L_{4-x} that relays the ST wave packet to an output plane after introducing an appropriate demagnification along the x -direction. In the Fourier plane between the lenses L_{3-x} and L_{4-x}, a spatial filter (SF₁) in the form of a thin wire is placed to reject low-pass spatial frequencies and thus remove the unwanted DC components (corresponding to plane waves propagating in the direction of the optical axis) that result from the finite diffraction efficiency of the SLM. The beam profile after the telescope system is recorded by a CCD camera (CCD₁; the Imaging Source, DMK 33UX178), which corresponds to a time-averaged intensity at a fixed plane z , $I(x, y, z) = \int dt |E(x, y, z, t)|^2$. The intensity is uniform along y for a width of ~ 25 mm, and we average the central portion of the beam over a width of $\Delta y \sim 1.32$ mm, $I(x, z) = \int_{\Delta y} dy I(x, y, z)$. The axial evolution of the time-averaged intensity $I(x, z)$ is recorded by scanning CCD₁ along z . This system is utilized with the ST wave packets and the separable pulsed beams.

4. Measuring the spatio-temporal spectra of ST wave packets

To characterize the spatio-temporal spectrum of the ST wave packets, a portion of the beam retro-reflected

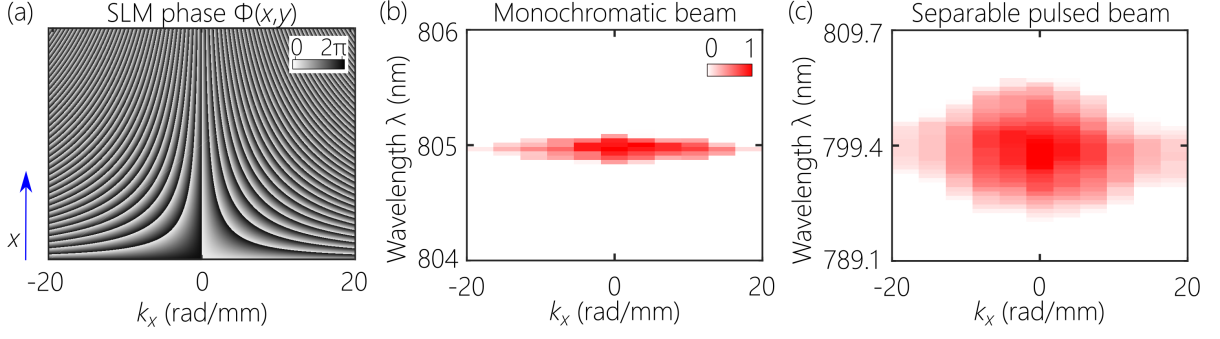


FIG. 8. (a) Implemented 2D SLM phase distribution $\Phi(x, y)$ to produce monochromatic and separable pulsed beams; $\Delta k_x = 20$ rad/mm. (b) Measured spatio-temporal spectrum $|\tilde{E}(k_x, \lambda)|^2$ for a monochromatic beam, corresponding to Fig. 1(a); and (c) for a separable pulsed beam having $\Delta\lambda = 8.5$ nm, corresponding to Fig. 1(b).

back from the SLM – after passing the lens L_{1-y} , but before reaching the diffraction grating G – is directed by a beam splitter (BS₂) through a spherical lens L_{2-s} ($f = 7.5$ cm) to a CCD camera (CCD₂; The Imaging Source, DMK 72AUC02) that is placed in the focal plane of L_{2-s} . The distance between the cylindrical lens L_{1-y} and the spherical lens L_{1-s} is designed such that they correspond to a $4f$ imaging configuration along the y -direction, such that the wavelengths are mapped from the SLM plane to the CCD plane. On the other hand, the spatial frequencies along the x -direction undergo a Fourier transform via L_{1-s} and are unaffected by L_{1-y} . Each spatial frequency at the SLM plane is thus mapped to a point in the CCD plane, thereby revealing the spatial spectrum. The intensity pattern recorded by CCD₂ therefore corresponds to the spatio-temporal spectrum $|\tilde{E}(k_x, \lambda)|^2$. The unwanted DC spectral components due to the finite diffraction efficiency of the SLM is removed by a spatial filter SF₂ placed in the Fourier plane between the lenses L_{1-y} and L_{2-s} (similarly to SF₁ at the output); see Fig. 7(a). This spatial filter is removed when synthesizing Class-2 wave packets ($\theta = 45^\circ$), which corresponds to a plane wave. The temporal spectral resolution of the measurement is limited by the pixel size of CCD₂. To obtain an accurate estimate of the spectral uncertainty $\delta\lambda$, we measure it via an optical spectrum analyzer (Advantest Q8384).

When a monochromatic or separable pulsed beam is synthesized in absence of G, we modify the spatio-temporal spectral measurement system as shown in Fig. 7(b). We make use of the same lens L_{2-s} after reflection from the beam-splitter BS₂, but then replace CCD₂ with a single-mode fiber at the focal plane of L_{2-s} . Each transverse position corresponds to a particular k_x . The fiber is scanned in the transverse plane, and the captured light is delivered to an optical spectrum analyzer (OSA, Advantest Q8384) that records the temporal spectrum at each position of the fiber tip.

B. Measurements results for monochromatic beams and separable pulsed beams

We first carried out measurements for a monochromatic beam and a traditional pulsed beam with separable spatial and temporal degrees of freedom. The monochromatic beam is produced from a CW laser diode (Thorlabs, CPS808S), which operates in the wavelength range 804–806 nm over a temperature range 20–25 °C and has a bandwidth of < 0.2 nm. The SLM phase pattern $\Phi(x, y)$ utilized is shown in Fig. 8(a). The right and left halves correspond to positive- and negative-valued spatial frequencies. In this way, the whole spatial spectrum is assigned to the quasi-monochromatic beam, and the spatio-temporal spectrum ideally is $\tilde{E}(k_x, \lambda) = \tilde{E}(k_x)\delta(\lambda - \lambda_0)$, which is separable in the spatial and temporal degrees of freedom; here $\tilde{E}(k_x)$ is the spatial spectrum and λ_0 is a fixed wavelength. The measured spatio-temporal spectrum obtained via the configuration in Fig. 7(b) is plotted in Fig. 8(b) confirming its separability.

The measurement was then carried out after replacing the CW laser with the Ti:Sa femtosecond laser, which was directed to the SLM with the phase pattern shown in Fig. 8(a) without first spectrally resolving the pulse. As a result, every wavelength in the pulse spectrum is now associated with the full spatial spectrum $\tilde{E}(k_x)$. Therefore, the spatio-temporal spectrum ideally takes the separable form $\tilde{E}(k_x, \lambda) = \tilde{E}_x(k_x)\tilde{E}_t(\lambda)$, where \tilde{E}_x and \tilde{E}_t are the spatial and temporal spectra, respectively. The measured spatio-temporal spectrum is shown in Fig. 8(c), confirming its separability. Neither the monochromatic beam nor the separable pulsed beam incorporate any spatio-temporal spectral correlations, and we thus expect that both will undergo diffractive spreading, as we confirm below.

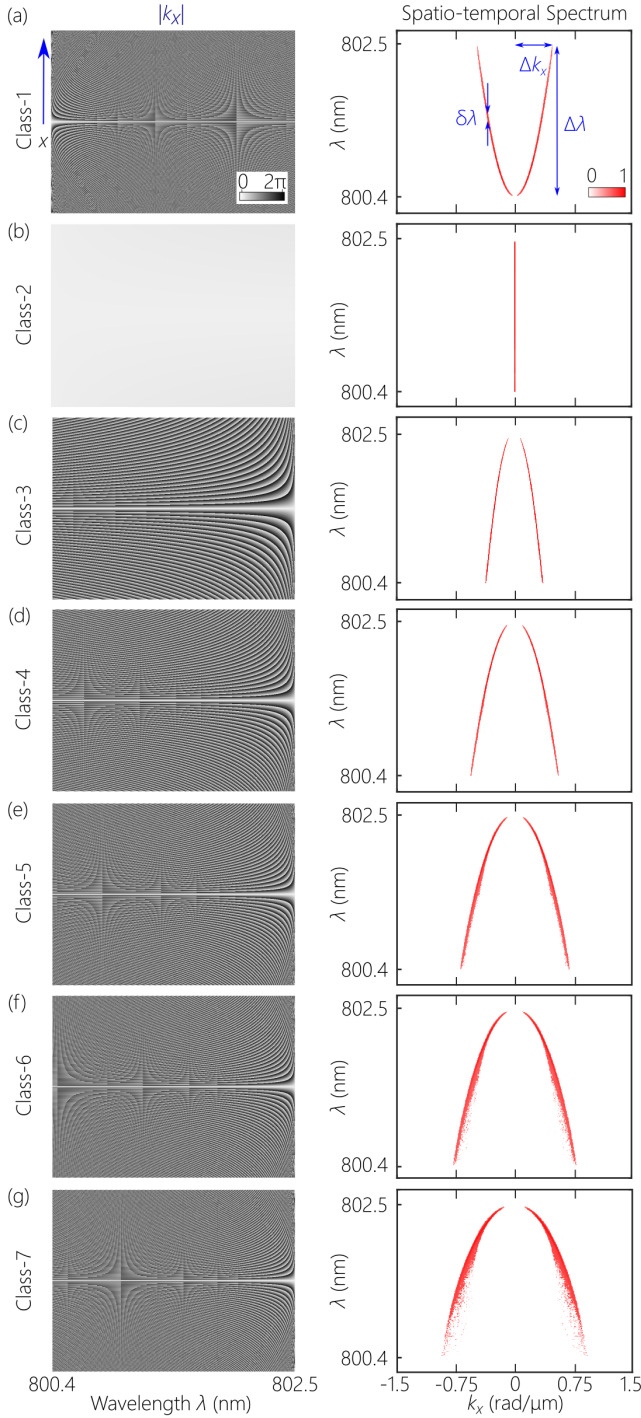


FIG. 9. Implemented 2D SLM phase distributions $\Phi(x, y)$ (left column) and measured spatio-temporal spectra $|\tilde{E}(k_x, \lambda)|^2$ (right column) for baseband ST wave packets, Class-1 through Class-7, as listed in Table III and depicted in Fig. 4. The temporal bandwidth for all classes is $\Delta\lambda = 2.1$ nm. (a) Class-1 with $\theta = 30^\circ$ and $\Delta k_x = 0.48$ rad/ μm ; (b) Class-2 with $\theta = 45^\circ$ and $\Delta k_x = 0$ rad/ μm ; (c) Class-3 with $\theta = 60^\circ$ and $\Delta k_x = 0.36$ rad/ μm ; (d) Class-4 with $\theta = 90^\circ$ and $\Delta k_x = 0.56$ rad/ μm ; (e) Class-5 with $\theta = 120^\circ$ and $\Delta k_x = 0.7$ rad/ μm ; (f) Class-6 with $\theta = 135^\circ$ and $\Delta k_x = 0.79$ rad/ μm ; and (g) Class-7 with $\theta = 150^\circ$ and $\Delta k_x = 0.93$ rad/ μm .

C. Measurements of baseband ST wave packets

We now move on to the synthesis of *baseband* ST wave packets, Class-1 through Class-7. The 2D phase distribution utilized for synthesizing representatives of these 7 classes and the corresponding measured spatio-temporal spectra $|\tilde{E}(k_x, \lambda)|^2$ – obtained by CCD₂ in Fig. 7(a) – are plotted in Fig. 9. The values of θ realized are: $\theta = 30^\circ$ (Class-1), 45° (Class-2), 60° (Class-3), 90° (Class-4), 120° (Class-5), 135° (Class-6), and 150° (Class-7). In all cases we maintain the same temporal bandwidth of $\Delta\lambda \sim 2.1$ nm. As a consequence of the spatio-temporal spectral correlations, changing θ at fixed $\Delta\lambda$ results in a corresponding change of the spatial bandwidth Δk_x from one class to the next, which is clear in the measured spectra shown in Fig. 9. The transverse spatial width of the ST wave packets will also change accordingly. Note that the measured spatio-temporal spectra are segments from the theoretically predicted conic sections: Fig. 9(a,g) are ellipses, Fig. 9(b) is a tangential line, Fig. 9(c-e) are hyperbolas, and Fig. 9(f) is a parabola. They are all *approximately* parabolas because of the limited Δk_x utilized.

Several observations are useful in interpreting the phase patterns $\Phi(x, y)$ in Fig. 9. First, as the spatial bandwidth Δk_x is increased, higher spatial variations in $\Phi(x, y)$ are required. This is particularly clear in Class-6 and Class-7 in Figs. 9(f,g). Second, the sign of the curvature of the spatio-temporal spectrum in the vicinity of $k_x = 0$ determines the orientation of $\Phi(x, y)$. In Fig. 9(a) for Class-1, the minimum wavelength is associated with $k_x = 0$ and higher k_x are associated with longer wavelengths. As such, the constant phase corresponding to $k_x = 0$ is located on the left (short wavelengths). Class-3 through Class-7 have the opposite curvature compared to Class-1, and thus the constant phase corresponding to $k_x = 0$ is located on the right (long wavelengths). Third, because Class-2 wave packets are pulsed plane waves, the needed $\Phi(x, y)$ is a constant [Fig. 4(b)]. Therefore, the initial spatial bandwidth of the incident large-area beam remained unchanged. Finally, in contrast to $\Phi(x, y)$ in Fig. 8(a) utilized in synthesizing the monochromatic and separable pulsed beams, the positive and negative values of k_x are arranged in the upper and lower halves of $\Phi(x, y)$, respectively.

The spectral uncertainty $\delta\lambda$ is ~ 30 pm, and we thus expect that all the synthesized ST wave packets will be quasi-diffraction-free over an axial propagation distance of ~ 15 mm [49].

D. Measurements of sideband ST wave packets

We report in Fig. 10 the measured spatio-temporal spectra for the synthesized *sideband* ST wave packets, Class-8 through Class-10. The 2D phase distribution $\Phi(x, y)$ utilized for synthesizing representatives of these 3 classes and the corresponding measured spatio-temporal spectrum $|\tilde{E}(k_x, \lambda)|^2$ are plotted in Fig. 10. The values

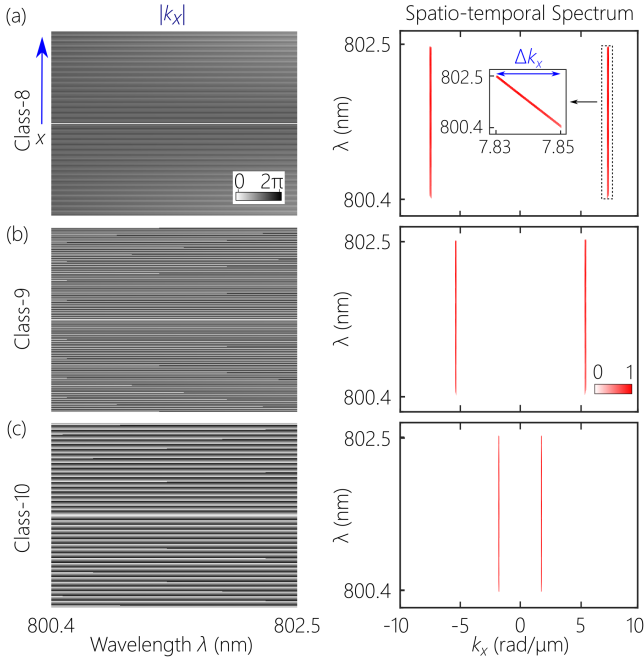


FIG. 10. SLM phase distributions $\Phi(x, y)$ and spatio-temporal spectra $|\tilde{E}(k_x, \lambda)|^2$ for sideband ST wave packets; $\Delta\lambda = 2.1$ nm throughout. (a) Class-8 with $\theta = 45^\circ$ and $\Delta k_x = 0.02$ rad/ μm ; (b) Class-9 with $\theta = 46^\circ$ and $\Delta k_x = 0.01$ rad/ μm ; (c) Class-10 with $\theta = 46^\circ$ and $\Delta k_x = 0.01$ rad/ μm . In all three classes, the spatial bandwidth Δk_x is very small and not easily resolvable. The inset in (a) is one branch of the spatio-temporal spectrum to show the extent of the spatial bandwidth.

of the tilt angle θ realized are: $\theta = 45^\circ$ (Class-8), 46° (Class-9), and 46° (Class-10).

We maintain the same temporal bandwidth of $\Delta\lambda \sim 2.1$ nm as in the case of baseband ST wave packets. The spatial frequencies involved in the sideband ST wave packets are significantly higher than those of the baseband counterparts for the same wavelengths. Note that the measured spatio-temporal spectra are segments from the theoretically predicted conic sections: Fig. 10(a) is a parabola, Fig. 10(b) is a hyperbola, and Fig. 10(c) a pair of lines. Because of the high k_x , however, the slopes of all the spatio-temporal spectra appear linear. Referring to the phase distributions $\Phi(x, y)$ in Fig. 10, first note the absence of the constant phase of $k_x = 0$ and of the slowly varying phases associated with low k_x – as expected in sideband ST wave packets in which the vicinity of $k_x = 0$ is excluded. Second, the spatial variation in $\Phi(x, y)$ for sideband classes is much more rapid than for baseband classes shown in Fig. 9 because of the large values of k_x involved. Third, because sideband ST wave packets are restricted to the range $\frac{\pi}{4} < \theta < \frac{\pi}{2}$, the left-right orientation $\Phi(x, y)$ is always the same.

E. Measurements of the axial propagation

Finally, we present measurements of the axial evolution of ST wave packets. First, we plot for the sake of comparison in Fig. 11(a) the time-averaged intensity distribution $I(x, z)$ for the *separable* pulsed beam captured by CCD₁ as it is scanned along the z -axis [Fig. 7]. As expected, diffractive spreading occurs away from the beam waist and the predicted Rayleigh range of $z_R = 4.8$ mm associated with a transverse spatial beam width of $\Delta x = 35$ μm is observed. A similar evolution is observed for the monochromatic beam that has the same spatial spectrum as the separable pulsed beam and hence the same beam width.

A wholly different behavior emerges once spatio-temporal spectral correlations are introduced in the synthesis of ST wave packets. We show in Fig. 11(b) the axial evolution of a Class-1 ST wave packet at $\theta = 30^\circ$ – corresponding to the spatio-temporal spectrum in Fig. 9(a), and in Fig. 11(c) that of a Class-3 ST wave packet at $\theta = 60^\circ$ – corresponding to the spatio-temporal spectrum in Fig. 9(c). We note first that the transverse beam profile is similar in both as a result of using the same incident femtosecond laser beam. Indeed, representatives for all the other baseband ST wave packets featured the same beam profile. Note that the larger spatial bandwidth Δk_x employed with respect to the separable pulsed beam has produced a smaller beam width Δx , as expected, but a *larger* propagation distance. Second, the sole observable difference is a change in the beam width Δx which varies inversely with Δk_x and depends on θ , as confirmed in Figs. 11(b,c).

VI. DISCUSSION

A. Justification for the classification

Our notation differs slightly from that adopted in the ‘slow-light’ and ‘fast-light’ literature, where term ‘fast-light’ has been used for materials or structures in which light travels with $v_g > c$ or $v_g < 0$. Here we have introduced quantitative distinctions to delineate the *magnitude* of v_g (for which we retain the terms subluminal, luminal, and superluminal) and its *direction* (positive or forward $v_g > 0$, and negative or backward $v_g < 0$). We find this apt because we can readily change either the magnitude or sign of v_g *independently* in our experiment by smoothly varying θ .

Our classification admits in principle $3 \times 2 \times 3 = 18$ classes of ST wave packets, of which 9 are eliminated on physical grounds: (1) Luminal X-waves, which coincide with Class-2 of luminal plane-wave pulses; (2) subluminal X-waves cannot be synthesized with real k_z ; (3) negative subluminal, luminal, and superluminal X-waves, which all correspond to $k_z < 0$; (4) positive subluminal sideband ST wave packets, which coincide with Class-1 positive subluminal *baseband* ST wave packets through the trans-

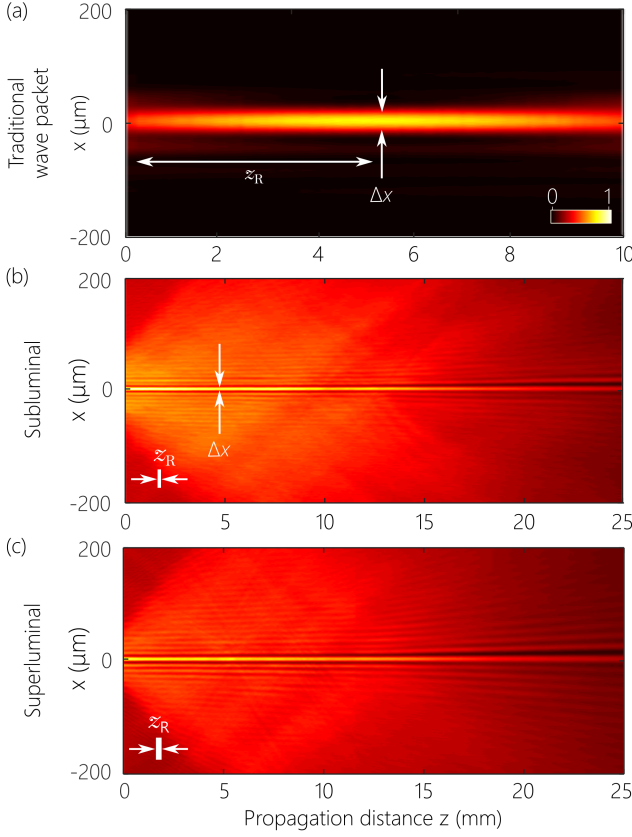


FIG. 11. Measured axial evolution of the time-averaged intensity $I(x, z)$ for (a) a separable pulsed beam having $\Delta\lambda = 8.5$ nm, $\Delta k_x = 0.09$ rad/ μm , and $\Delta x = 35$ μm , corresponding to Fig. 8(c); (b) a Class-1 ST wave packet with $\theta = 30^\circ$, $\Delta\lambda = 2.1$ nm, $\Delta k_x = 0.48$ rad/ μm , and $\Delta x = 6$ μm , corresponding to Fig. 9(a); and (c) a Class-3 ST wave packet with $\theta = 60^\circ$, $\Delta\lambda = 2.1$ nm, $\Delta k_x = 0.36$ rad/ μm , and $\Delta x = 8$ μm , corresponding to Fig. 9(c). The Rayleigh range z_R associated with the transverse width Δx is identified graphically in each of the three cases, and are given by (a) 4.8 mm, (b) 150 μm , and (c) 250 μm . Note the different axial (horizontal) scale used in (a) with respect to (b) and (c).

formation in Eq. 30; and (5) negative subluminal, luminal, and superluminal sideband ST wave packets, which require $k_z < 0$. All these can be seen clearly by examining the geometric models in Fig. 4 and Fig. 6. Note that Class-4 of nominally infinite- v_g was listed separately for its interesting time-diffraction properties, although it is not logically an independent class (only a limit separating Class-3 and Class-5 of positive and negative- v_g , respectively). Finally, we associated X-waves with *sideband* ST wave packets because they share the same angular range of $\frac{\pi}{4} < \theta < \frac{\pi}{2}$ (negative- v_g is not allowed). In general, achieving these specifications of v_g is limited by the spectral uncertainty $\delta\lambda$, especially in the vicinity of $\theta = \frac{\pi}{2}$. We will present our measurements of v_g with θ elsewhere [67].

Most importantly, this categorization reveals some fun-

damental differences between the different classes of ST wave packets. For example, some classes are amenable to ultrawide temporal and spatial bandwidths (e.g., Class-3 through Class-5), while others have restrictions on the achievable bandwidths (e.g., Class-1, Class-6, and Class-7). Surprisingly, we find that the sign of the *phase* velocity determines whether low spatial frequencies are allowable. As such, *baseband* ST wave packets (Class-1 through Class-7) are associated with *positive- v_{ph}* , whereas *sideband* ST wave packets (Class-8 and Class-9) are associated with *negative- v_{ph}* . Moreover, *only* baseband ST wave packets (specifically, Class-5 through Class-7) can achieve negative group velocities. Finally, we have found that Class-1 ST wave packets allow a two-to-one association between $|k_x|$ and ω in some range of spatial frequencies, whereas all other classes maintain a one-to-one correspondence.

B. Further developments

The conceptual and theoretical framework outlined here can be developed in a variety of directions and indeed helps show the intersection of the study of ST wave packets with other recently investigated topics in optical physics.

In this paper we have discussed ST wave packets that are (2+1)D, and thus have the form of a light sheet. Previously examined propagation-invariant wave packets [8, 29] have been (3+1)D. An important question is whether the classification presented here extends to the (3+1)D case or whether new classes emerge. We conjecture that the current classification is in fact exhaustive since the transition from the (2+1)D case to the (3+1)D case involves exchanging the spatial frequency $|k_x|$ for the 2D transverse spatial frequency $k_T = (k_x^2 + k_y^2)^{1/2}$. However, it is not clear at the moment how the experimental strategy described here can be extended to the synthesis of (3+1)D wave packets.

It is important to point out here the relationship between the study of ST wave packets and that of ‘classical entanglement’, which is the analog of multi-partite quantum entanglement applied to the correlations between the different degrees of freedom of a classical optical field [82–86]. This concept has found applications in optical coherence theory [83, 87] and in tracking the kinematics of fast-moving particles [88]. In all studies of classical entanglement to date, correlations between *discretized* degrees of freedom, such as polarization and spatial modes, have been investigated. ST wave packets are the first example of controllably introducing correlations or classical entanglement between continuous degrees of freedom, spatial and temporal frequencies.

We have examined (2+1)D ST wave packets whose spatio-temporal spectra lie along reduced-dimensionality trajectories on the surface of the light cone – specifically 1D curves at the intersection of the light-cone with tilted spectral hyperplanes. Recently, we have demon-

strated that the tilting of these spectral hyperplanes can be viewed as the result of relativistic Lorentz transformations associated with frames moving with respect to the source [46]. Thus, transitioning from one class to another in our classification can be viewed as the result of a Lorentz boost; see also Refs. [30, 31, 89]. In this sense, the ability to controllably synthesize ST wave packets opens up avenues for laboratory-scale studies of relativistic optical effects [90].

Although we have focused here on coherent pulsed fields, as is also the case in previous literature, there is nothing to prevent implementing all these classes of ST wave packets using broadband incoherent light instead. Indeed, a first study along this line has demonstrated that the intensity of a broadband incoherent ST field is diffraction-free [51]. One may now consider the 10 classes studied here in the context of incoherent ST fields, whereupon the ‘speed of coherence’ can be controlled above or below c in free space.

Finally, we briefly discuss other directions of future research. First, nonlinear correlation functions relating ω to k_z are yet to be explored, which do *not* result from the intersection of the light-cone with a spectral hyperplane, but instead with non-planar surfaces. Second, the propagation of ST wave packets in optical materials including dispersive media has received previous attention, but may appear in a different light within the framework described here. Additionally, the study of the propagation of ST wave packets in nonlinear media appears promising [91]. Most interesting would be exploring the nature of light-matter interactions when ST wave packets of controllable- v_g are brought into contact with dielectric

micro- and nanoparticles or charged particles.

VII. CONCLUSIONS

In conclusion, we have presented a comprehensive theoretical and experimental classification of all $(2+1)D$ propagation-invariant ST wave packets in free space. In constructing this classification, we have made use of three criteria: the magnitude of the group velocity (subluminal, luminal, or superluminal); the sign of the group velocity (positive or negative); and whether the ST wave packet is ‘baseband’ or ‘sideband’ – whether low spatial frequencies are allowed or forbidden, respectively. This classification reveals 10 distinct classes that we have described in detail and synthesized experimentally using an optical arrangement that combines spatial beam-modulation with ultrafast pulse-shaping. We have eschewed the traditional *analytic* approach whereby specific solutions for the appropriate wave equation are sought, and have instead adopted a *synthetic* strategy whereby an arbitrary spectrum is utilized in the wave packet’s plane-wave expansion. This approach amounts to a realization of *spatio-temporal Fourier optics* applied to the problem of synthesizing propagation-invariant wave packets.

ACKNOWLEDGMENTS

We thank D. Mardani, G. K. Atia, D. N. Christodoulides, and A. Dogariu for useful discussions. This work was supported by the U.S. Office of Naval Research (ONR) under contract N00014-17-1-2458.

-
- [1] G. B. Airy, Phil. Mag. **318**, 1 (1841).
 - [2] J. W. S. Rayleigh, Mon. Not. R. Astron. Soc. **33**, 59 (1872).
 - [3] G. C. Steward, Philos. Trans. R. Soc. London (Ser. A) **225**, 131 (1926).
 - [4] J. Stratton, *Electromagnetic Theory* (McGraw-Hill, New York, 1941).
 - [5] W. H. Steel, Rev. Opt. **32**, 143 (1953).
 - [6] W. T. Welford, J. Opt. Soc. Am. **50**, 749 (1960).
 - [7] C. J. R. Sheppard, Optik **48**, 329 (1977).
 - [8] H. E. Hernández-Figueroa, E. Recami, and M. Zamboni-Rached, eds., *Non-diffracting Waves* (Wiley-VCH, 2014).
 - [9] D. McGloin and K. Dholakia, Contemp. Phys. **46**, 15 (2005).
 - [10] M. Mazilu, D. Stevenson, F. Gunn-Moore, and K. Dholakia, Laser Photon. Rev. **4**, 529 (2010).
 - [11] J. Durnin, J. J. Miceli, and J. H. Eberly, Phys. Rev. Lett. **58**, 1499 (1987).
 - [12] M. A. Bandres, J. C. Gutiérrez-Vega, and S. Chávez-Cerda, Opt. Lett. **29**, 44 (2004).
 - [13] B. M. Rodríguez-Lara, J. Opt. Soc. Am. A **27**, 327 (2010).
 - [14] G. A. Siviloglou, J. Broky, A. Dogariu, and D. N. Christodoulides, Phys. Rev. Lett. **99**, 213901 (2007).
 - [15] U. Levy, S. Derevyanko, and Y. Silberberg, Prog. Opt. **61**, 237 (2016).
 - [16] M. V. Berry and N. L. Balazs, Am. J. Phys. **47**, 264 (1979).
 - [17] G. A. Siviloglou and D. N. Christodoulides, Opt. Lett. **32**, 979 (2007).
 - [18] J. N. Brittingham, J. Appl. Phys. **54**, 1179 (1983).
 - [19] L. Mackinnon, Found. Phys. **8**, 157 (1978).
 - [20] J.-Y. Lu and J. F. Greenleaf, IEEE Trans. Ultrason. Ferroelec. Freq. Control **39**, 19 (1992).
 - [21] J.-Y. Lu and J. F. Greenleaf, IEEE Trans. Ultrason. Ferroelec. Freq. Control **39**, 441 (1992).
 - [22] P. Saari and K. Reivelt, Phys. Rev. Lett. **79**, 4135 (1997).
 - [23] I. M. Besieris, A. M. Shaarawi, and R. W. Ziolkowski, J. Math. Phys. **30**, 1254 (1989).
 - [24] A. Wünsche, J. Opt. Soc. Am. A **6**, 1661 (1989).
 - [25] R. Donnelly and R. Ziolkowski, Proc. R. Soc. Lond. A **440**, 541 (1993).
 - [26] I. Besieris, M. Abdel-Rahman, A. Shaarawi, and A. Chatzipetros, Progr. in Electrom. Res. **19**, 1 (1998).
 - [27] J. Salo, J. Fagerholm, A. T. Friberg, and M. M. Salomaa, Phys. Rev. E **62**, 4261 (2000).
 - [28] C. J. R. Sheppard, J. Opt. Soc. Am. A **19**, 2218 (2002).
 - [29] J. Turunen and A. T. Friberg, Prog. Opt. **54**, 1 (2010).

- [30] S. Longhi, *Opt. Express* **12**, 935 (2004).
- [31] P. Saari and K. Reivelt, *Phys. Rev. E* **69**, 036612 (2004).
- [32] H. E. Kondakci and A. F. Abouraddy, *Opt. Express* **24**, 28659 (2016).
- [33] H. E. Kondakci and A. F. Abouraddy, *Nat. Photon.* **11**, 733 (2017).
- [34] K. J. Parker and M. A. Alonso, *Opt. Express* **24**, 28669 (2016).
- [35] H. Sönaialg, M. Rätsep, and P. Saari, *Opt. Lett.* **22**, 310 (1997).
- [36] M. A. Porras, *Opt. Lett.* **26**, 1364 (2001).
- [37] S. Orlov, A. Piskarskas, and A. Stabinis, *Opt. Lett.* **27**, 2167 (2002).
- [38] B. Lü and Z. Liu, *J. Opt. Soc. Am. A* **20**, 582 (2003).
- [39] D. N. Christodoulides, N. K. Efremidis, P. Di Trapani, and B. A. Malomed, *Opt. Lett.* **29**, 1446 (2004).
- [40] S. Longhi, *Opt. Lett.* **29**, 147 (2004).
- [41] M. Dallaire, N. McCarthy, and M. Piché, *Opt. Express* **17**, 18148 (2009).
- [42] M. S. Mills, G. A. Siviloglou, N. Efremidis, T. Graf, E. M. Wright, J. V. Moloney, and D. N. Christodoulides, *Phys. Rev. A* **86**, 063811 (2012).
- [43] O. Jedrkiewicz, Y.-D. Wang, G. Valiulis, and P. Di Trapani, *Opt. Express* **21**, 25000 (2013).
- [44] P. Di Trapani, G. Valiulis, A. Piskarskas, O. Jedrkiewicz, J. Trull, C. Conti, and S. Trillo, *Phys. Rev. Lett.* **91**, 093904 (2003).
- [45] E. DelRe, F. Di Mei, J. Parravicini, G. Parravicini, A. J. Agranat, and C. Conti, *Nat. Photon.* **9**, 228 (2015).
- [46] H. E. Kondakci and A. F. Abouraddy, *Phys. Rev. Lett.* **120**, 163901 (2018).
- [47] H. E. Kondakci, M. Yessenov, M. Meem, D. Reyes, D. Thul, S. R. Fairchild, M. Richardson, R. Menon, and A. F. Abouraddy, *Opt. Express* **26**, 13628 (2018).
- [48] H. E. Kondakci and A. F. Abouraddy, *Opt. Lett.* **43**, 3830 (2018).
- [49] B. Bhaduri, M. Yessenov, and A. F. Abouraddy, *Opt. Express* **26**, 20111 (2018).
- [50] B. Bhaduri, M. Yessenov, D. Reyes, J. Pena, M. Meem, S. R. Fairchild, R. Menon, M. C. Richardson, and A. F. Abouraddy, submitted (2018).
- [51] M. Yessenov, B. Bhaduri, H. E. Kondakci, M. Meem, R. Menon, and A. F. Abouraddy, submitted (2018).
- [52] L. J. Wong and I. Kaminer, *ACS Photon.* **4**, 1131 (2017).
- [53] L. J. Wong and I. Kaminer, *ACS Photon.* **4**, 2257 (2017).
- [54] M. A. Porras, *Opt. Lett.* **42**, 4679 (2017).
- [55] A. Sainte-Marie, O. Gobert, and F. Quéré, *Optica* **4**, 1298 (2017).
- [56] N. K. Efremidis, *Opt. Lett.* **42**, 5038 (2017).
- [57] M. A. Porras, *Phys. Rev. A* **97**, 063803 (2018).
- [58] E. Heyman, B. Z. Steinberg, and L. B. Felsen, *J. Opt. Soc. Am. A* **4**, 2081 (1987).
- [59] E. Heyman, *IEEE Trans. Antennas Propag.* **37**, 1604 (1989).
- [60] E. Heyman, in *Ultra-Wideband, Short-Pulse Electromagnetics*, edited by H. L. Bertoni, L. Carin, and L. B. Felsen (Springer, Boston, 1993).
- [61] A. M. Shaarawi, R. W. Ziolkowski, and I. M. Besieris, *J. Math. Phys.* **36**, 5565 (1995).
- [62] G. Pariente, V. Gallet, A. Borot, O. Gobert, and F. Quéré, *Nat. Photon.* **10**, 547 (2016).
- [63] B. E. A. Saleh and M. C. Teich, *Principles of Photonics* (Wiley, 2007).
- [64] P. A. Bélanger, *J. Opt. Soc. Am. A* **1**, 723 (1984).
- [65] J. Salo and M. M. Salomaa, *J. Opt. A* **3**, 366 (2001).
- [66] R. L. Garay-Avendaño and M. Zamboni-Rached, *Appl. Opt.* **55**, 1786 (2016).
- [67] H. E. Kondakci and A. F. Abouraddy, unpublished (2018).
- [68] R. L. Smith, *Am. J. Phys.* **38**, 978 (1970).
- [69] W. C. Salmon, *Four Decades of Scientific Explanation* (Univ. Pittsburgh Press, 2006).
- [70] P. Saari, *Phys. Rev. A* **97**, 063824 (2018).
- [71] H. Valtna, K. Reivelt, and P. Saari, *Opt. Commun.* **278**, 1 (2007).
- [72] K. Reivelt and P. Saari, *J. Opt. Soc. Am. A* **17**, 1785 (2000).
- [73] K. Reivelt and P. Saari, *Phys. Rev. E* **66**, 056611 (2002).
- [74] A. M. Weiner, *Rev. Sci. Instrum.* **71**, 1929 (2000).
- [75] A. M. Weiner, *Ultrafast Optics* (John Wiley & Sons, Inc., 2009).
- [76] R. M. Koehl, T. Hattori, and K. A. Nelson, *Opt. Commun.* **157**, 57 (1998).
- [77] T. Feurer, J. C. Vaughan, R. M. Koehl, and K. A. Nelson, *Opt. Lett.* **27**, 652 (2002).
- [78] T. Tanab, F. Kannari, F. Korte, J. Koch, and B. Chichkov, *Appl. Opt.* **44**, 1092 (2005).
- [79] G. Zhu, J. van Howe, M. Durst, W. Zipfel, and C. Xu, *Opt. Express* **13**, 2153 (2005).
- [80] B. J. Sussman, R. Lausten, and A. Stolow, *Phys. Rev. A* **77**, 043416 (2008).
- [81] F. He, B. Zeng, W. Chu, J. Ni, K. Sugioka, Y. Cheng, and C. G. Durfee, *Opt. Express* **22**, 9734 (2014).
- [82] X.-F. Qian and J. H. Eberly, *Opt. Lett.* **36**, 4110 (2011).
- [83] K. H. Kagalwala, G. Di Giuseppe, A. F. Abouraddy, and B. E. A. Saleh, *Nat. Photon.* **7**, 72 (2013).
- [84] A. F. Abouraddy, K. H. Kagalwala, and B. E. A. Saleh, *Opt. Lett.* **39**, 2411 (2014).
- [85] A. Aiello, F. Töppel, C. Marquardt, E. Giacobino, and G. Leuchs, *New J. Phys.* **17**, 043024 (2015).
- [86] K. H. Kagalwala, H. E. Kondakci, A. F. Abouraddy, and B. E. A. Saleh, *Sci. Rep.* **5**, 15333 (2015).
- [87] C. Okoro, H. E. Kondakci, A. F. Abouraddy, and K. C. Toussaint, *Optica* **4**, 1052 (2017).
- [88] S. Berg-Johansen, F. Töppel, B. Stiller, P. Banzer, M. Ornigotti, E. Giacobino, G. Leuchs, A. Aiello, and C. Marquardt, *Optica* **2**, 864 (2015).
- [89] P. A. Bélanger, *J. Opt. Soc. Am. A* **3**, 541 (1986).
- [90] K. Y. Bliokh and F. Nori, *Phys. Rev. A* **86**, 033824 (2012).
- [91] M. A. Porras, arXiv:1805.07985 (2018).